Gene-Gene Interactions Between A *LMNA* Variant and Common Polymorphisms Drive Early-Onset Atrial Fibrillation

Asia Owais[1], Hammad Farooq[2,3], Hannah Chen[1], Prisca K Thami[4,5], Jaime DeSantiago[1], Talla Abbas[6], Arif Pavel[1], Bradley Merril[6]

James S Ware[4,5,7,8], Fu Siong Ng[4], Dawood Darbar[1,9]

[1]Department of Medicine, Division of Cardiology, University of Illinois Chicago, Chicago, IL. [2]Center for Bioinformatics and Quantitative Biology, University of Illinois Chicago, Chicago, IL. [3]Richard and Loan Hill Department of Biomedical Engineering, University of Illinois Chicago, Chicago, IL. [4]National Heart and Lung Institute, Imperial College London, London, UK. [5]MRC Laboratory of Medical Sciences, Imperial College London, London, UK. [6]Department of Biochemistry & Molecular Genetics, University of Illinois Chicago; [7] Royal Brompton & Harefield Hospitals, Guy's and St. Thomas' NHS Foundation Trust, London, UK; [8]Program in Medical and Population Genetics, The Broad Institute of MIT and Harvard, Cambridge, MA, USA; [9]Department of Medicine, Jesse Brown Veterans Administration, Chicago, IL, USA.

Address correspondence to:
Dawood Darbar, MD
Department of Medicine
University of Illinois Chicago
Chicago, IL 60614
email: darbar@uic.edu

Abstract

Atrial fibrillation (AF) is a common arrhythmia with a complex genetic basis, yet the molecular mechanisms linking rare and common variants remain unclear. Using induced pluripotent stem cell-derived atrial cardiomyocytes, we uncover a novel mechanism by which a rare pathogenic *LMNA* variant encoding Lamin A/C disrupts chromatin accessibility and gene regulation at AF-associated loci. Specifically, reduced accessibility at an *SCN5A* enhancer harboring an AF-associated variant leads to reduced sodium current, conduction abnormalities, and re-entrant AF. These electrophysiological defects are rescued by CRISPR-mediated activation of the *SCN5A* promoter and enhancer, providing the first molecular evidence of epistatic gene-gene interactions driving arrhythmia risk and mechanistically linking atrial myopathy and AF. At the population level, we demonstrate that carriers of *LMNA* protein-altering variants with a high polygenic risk score are at a two-fold increased risk of early-onset AF, highlighting the need to integrate rare and common variants for more accurate AF risk assessment.

Introduction

Atrial fibrillation (AF) is the most common cardiac arrhythmia worldwide and has a strong genetic basis[1]. Both rare and common genetic variants contribute to AF susceptibility[2]. Genome-wide association studies (GWAS) have identified numerous common variants associated with AF, whereas whole genome and whole exome sequencing studies have uncovered individually rare, high-impact variants[3,4]. The development of polygenic risk scores (PRS) has improved AF risk prediction, with emerging evidence suggesting that common variants can modulate the penetrance of rare monogenic variants[4-6]. However, the molecular mechanisms underlying these gene-gene interactions and their role in creating an arrhythmogenic substrate remain poorly understood. A deeper understanding of these epistatic interactions could open new avenues for precision medicine and improve risk stratification.

Variants in *LMNA*, which encodes the nuclear envelope protein Lamin A/C, are implicated in a spectrum of disorders, including isolated cardiac disease[7]. Clinically, *LMNA* mutations are associated with conduction system disease, AF, ventricular arrhythmias, and dilated cardiomyopathy (DCM)[7]. AF is a particularly common and early manifestation in *LMNA*-associated cardiomyopathy[3,8-10]. Lamin A/C, as type V intermediate filaments, play critical roles in cytoskeletal and nuclear structural integrity, chromatin organization, and gene regulation. *LMNA* variants can disrupt gene expression through epigenetic mechanisms, including altered chromatin accessibility and genome organization[4,11-13].

We hypothesized that a rare *LMNA* variant may alter chromatin accessibility and gene expression at AF-risk loci, unmasking the effects of common polymorphisms in cis-regulatory regions and thereby influencing AF susceptibility in carriers of protein-

altering variants (PAVs) in *LMNA*. To test this, we conducted chromatin accessibility and gene expression profiling in induced pluripotent stem cell-derived atrial cardiomyocytes (iPSC-aCMs) generated from a proband carrying the *LMNA*-S143P variant. This analysis identified significantly altered chromatin accessibility at eight AF-associated loci, including a single nucleotide polymorphism (SNP) within a known *SCN5A* enhancer[14]. SCN5A expression and sodium channel current (I_{Na}) were consistently reduced, impairing atrial conduction and promoting re-entry, thereby predisposing to early-onset AF (defined as AF occurring prior to 66 years)[8,15]. Gene expression changes at additional AF-associated loci identified via Promoter-Capture Hi-C (PC-Hi-C) further reinforced the role of epistatic interactions in AF susceptibility[16].

To investigate the functional relevance of these chromatin changes, we employed CRISPR-based approaches to correct the *LMNA*-S143P variant, activate the *SCN5A* promoter, and enhance *SCN10A* regulatory activity. These interventions successfully restored SCN5A expression and I_{Na}, confirming that chromatin remodeling at this AF-risk locus was a key driver of the observed electrophysiological (EP) defects. Our findings support a model in which epistatic interactions between a rare *LMNA* variant and common polymorphisms establish a pro-arrhythmic molecular substrate, contributing to AF pathogenesis.

Prior studies suggest that common variants modulate the penetrance of rare monogenic variants[4,6]. To determine the combined contribution of common polymorphisms and rare *LMNA* variants to AF risk, we applied a PRS for AF to carriers of rare *LMNA* PAVs in the UK Biobank and *All of Us* (AoU) cohorts. Individuals with a high PRS exhibited a two-fold increased risk of early-onset AF compared to those with

a lower PRS emphasizing the need to integrate rare and common genetic variations for improved AF risk stratification.

This study unveils a novel molecular mechanism through which epistatic gene-gene interactions drive early-onset AF in *LMNA* variant carriers. These findings highlight the need for comprehensive genetic assessment, incorporating both rare and common variants, not only for risk prediction but also for early intervention to prevent atrial myopathy and its complications, including stroke.

Results

Cardiac Phenotype of LMNA-S143P Kindred

The proband (III-3) developed early-onset AF in her 30s. She initially underwent direct current cardioversion to maintain sinus rhythm, but the persistence of symptomatic AF necessitated pulmonary vein ablation a year later. Notably, diffuse low-amplitude atrial electrograms were recorded during the ablation. The patient, however, continued to experience symptomatic persistent AF with bradycardia and underwent implantation of a biventricular pacemaker (**Table 1**). A transthoracic echocardiogram at the time of the ablation showed evidence of mild atrial myopathy but preserved left ventricular function with an ejection fraction of 56%. Cardiac magnetic resonance imaging also showed an enlarged left atrium but no evidence of DCM. A detailed family history revealed that multiple family members were affected by cardiovascular disease (**Fig. 1a**). Most family members started to experience symptoms in their mid-30s. The maternal grandmother (I-2) and several of her siblings died due to congestive heart failure (CHF). Three family members (II-2,II-6 and III-4) developed early-onset AF, while one family member (II-4) underwent heart transplantation due to CHF. The proband's maternal cousin (III-7) died of sudden death

in the 30's. Several family members have also undergone pacemaker implantation. Genetic testing of the proband confirmed the presence of a heterozygous missense pathogenic variant in the second exon of *LMNA*. A base substitution from Thymine to Cytosine results in an amino acid change from Serine to Proline (NM_170707.4(LMNA):c.427T>C [p.Ser143Pro]) (**Fig. 1b**). The variant is classified as "pathogenic" for DCM by the American College of Medical Genetics and Genomics guidelines[17,18]. It is also the most prevalent variant in *LMNA* associated with DCM in Finland[19,20]. Genetic testing of the affected mother (II-2) confirmed that she also harbored the *LMNA*-S143P variant, while cascade screening determined that the the proband's sibling (III-2) was not a carrier.

To identify the molecular mechanisms by which epistatic rare-common variant interactions create a substrate for AF, we generated iPSCs from the proband, healthy control, and CRISPR corrected the mutation to generate an isogenic control labeled as *LMNA*-S143P, wild-type (WT), and *LMNA*-S143P-Corrected respectively. The iPSCs were differentiated into atrial cardiomyocytes and matured for four weeks before analysis. Protein expression analysis revealed reduced Lamin A/C levels in *LMNA*-S143P iPSC-aCMs compared to controls, suggesting haploinsufficiency caused by the mutant allele (**Fig. 1d**, **Supplementary Figs. 1-2**).

The LMNA-S143P variant causes extensive transcriptional changes and alters regulatory interactions in AF susceptibility genes

Lamins anchor chromatin to the nuclear periphery in transcriptionally inactive lamina-associated domains (LADs), while also interacting with transcriptionally active chromatin within the nucleoplasm[21]. Variants in *LMNA* can disrupt chromatin organization and influence gene expression through epigenetic mechanisms[22]. To investigate the alterations in gene expression due to altered chromatin contacts and accessibility, we performed gene expression and chromatin accessibility profiling using

RNA-sequencing (RNA-seq) and Assay for Transposase-Accessible Chromatin (ATAC)-seq of *LMNA*-S143P iPSC-aCMs and WT controls and cross-referenced with published Promoter Capture Hi-C (PC-Hi-C) data from iPSC-derived cardiomyocytes **(Fig. 1c)**[16].

Differential gene expression (DEG) analysis revealed extensive transcriptional changes, with 4,341 upregulated and 4,015 downregulated genes (**Fig. 2a**). Notably, genes critical for cardiac conduction were significantly altered, with marked downregulation of *SCN5A*, a key regulator of conduction strongly linked to early-onset AF[23,24] (**Fig. 2b**). Structural genes associated with early onset-AF such *as MYL4, TTN, MYBPC3, DSP* and *PKP2* were also significantly downregulated along with other cytoskeletal genes (**Fig. 2c-d)**[25] Gene enrichment identified altered cardiovascular signaling pathways, including upregulation of DCM, β-adrenergic signaling and downregulation of the cardiac hypertrophy and differentiation pathways (**Fig. 2e, Supplementary Figs. 4a-b**). The DNA damage repair pathway was also upregulated, alluding to the impact on the nucleus and chromatin due to impaired mechanical stress resilience of the Lamin A/C deficient nuclear lamina **(Fig.1d Supplementary Fig. 5** and **8).**

ATAC-seq-based chromatin accessibility profiling identified 44,981 differential chromatin accessibility peaks between the two groups, with 25,151 upregulated and 19,830 downregulated in *LMNA*-S143P iPSC-aCMs compared to WT. Notably, most of these differential peaks were in non-coding regions (**Fig. 2f**), suggesting that the widespread changes driven by the *LMNA*-S143P variant may result from its impact on cis-regulatory regions, such as enhancers or silencers. Chromatin accessibility changes at transcription start sites (TSS) of the majority (77%) of DEGs correlated positively with gene expression changes ($r = 0.75$; $p<0.0001$; **Fig. 2g**). Pathway analysis of genes with altered promoter accessibility revealed significant enrichment

in pathways related to cardiac development and repair, including, DCM, calcium signaling, and the Wnt signaling (**Fig. 2h**).

To further investigate changes in chromatin contacts in regulatory regions, we identified enhancers using published H3K27ac chromatin immunoprecipitation (ChIP)-seq data from human atrial tissue (ENCSR074ECR) and mapped their target genes by cross-referencing published PC-Hi C data[16]. Our analysis revealed significant alterations in chromatin contacts between promoters and enhancers in *LMNA*-S143P iPSC-aCMs. We found that there was a strong correlation of enhancer accessibility with differentially expressed target genes ($r=0.6856$, $r^2=0.47$, $p<0.0001$) (**Fig.3a**). Pathway analysis of the target genes of enhancer regions with altered accessibility showed enrichment for GO terms related to heart development and cytoskeletal reorganization (**Fig. 3b**). We found reduced accessibility at enhancers of genes encoding transcription factors, *TBX5, GATA4, GATA6*, and the atrial-specific gene, *NPPA* encoding atrial natriuretic peptide, a key signaling molecule secreted in response to atrial stretch (**Fig. 3c-g**). The concurrent reduction in the expression levels of these genes suggested altered promoter enhancer contacts. *GATA4, GATA6*, and *TBX5* encode transcription factors that work co-operatively to drive a gene expression program for cardiac development and have been implicated in conduction disorders and familial AF[3,26-30]. *TBX5* maintains an atrial enhancer network regulating atrial-specific genes[31]. We found downregulation of several known TBX5 transcriptional targets encoding ion channels, calcium signaling genes, and structural proteins (**Fig. 3h**)[31-33].

Overall, these results suggest that the gene expression changes in *LMNA*-S143P iPSC-aCMs are partly driven by altered chromatin contacts in regulatory regions of genes involved in atrial arrhythmogenesis, which may increase susceptibility to AF.

Chromatin accessibility at AF susceptibility loci is altered by the LMNA-S143P variant in iPSC-aCMs

To further understand the genetic mechanisms that predispose to early-onset AF, we hypothesized that altered accessibility at AF risk loci may modulate the AF phenotype in carriers of rare PAVs in *LMNA* through epistatic interactions. To test this hypothesis, we cross-referenced differential ATAC peaks with AF-associated risk loci identified by three recent AF-GWAS[26,34,35].

By overlapping GWAS AF risk loci with regions of significantly altered chromatin accessibility, we identified eight AF-associated loci (**Supplementary Table 1**). Notably, there was a significantly reduced accessibility at a region harboring the rs6801957 single nucleotide polymorphism (SNP) on chromosome 3 in the *SCN10A* gene, with *SCN5A* as the neighboring gene (**Fig. 4a, Supplementary Table 1**). *SCN10A* encodes the voltage-gated sodium channel Nav1.8 which is minimally expressed in the heart and is primarily expressed in neurons. *SCN5A-SCN10A* locus is a variant-sensitive region encompassing several variants associated with electrocardiographic traits[14,36]. The rs6801957 SNP is in an intronic region of *SCN10A*, a known enhancer region for *SCN5A*[14]. This suggests that alteration in chromatin accessibility at this locus may alter the promoter enhancer interaction leading to reduced expression of *SCN5A*. Expression analysis by qualitative polymerase chain reaction (qPCR) and Western blot showed reduced *SCN5A* mRNA and protein levels in *LMNA*-S143P iPSC-aCMs (**Fig. 4 e, f, Supplementary Fig. 5**). To confirm that SCN5A downregulation resulted from reduced transcription rather than proteolytic degradation, we analyzed the gene expression changes in autophagy and endoplasmic reticulum stress pathways involved in proteolysis. The absence of upregulated genes in these pathways supported that Nav1.5 downregulation occurred at the transcript level (**Supplementary Fig. 6**).

Since all the AF-associated SNPs overlapping with differentially accessible regions also overlap with H3K27ac peaks[16], a marker of active enhancers, we leveraged published PC-Hi-C data from iPSC-derived cardiomyocytes to identify the target genes of these enhancer regions[16]. This analysis revealed altered expression of several target genes implicated in AF pathogenesis (**Fig. 4b-e**). For instance, PC-Hi-C identified *CEP68* as the target gene of the region harboring the rs2540949 SNP. CEP68 was upregulated and is known to play a role in sinus node dysfunction (**Fig. 4b**)[37]. Similarly, Neuroplastin (*NPTN*), identified as the target gene of the region containing rs7172038, is expressed in atrial tissue and involved in atrial differentiation and regulation of heart rate. *NPTN* was significantly downregulated in *LMNA*-S143P iPSC-aCMs (**Fig. 4c**)[38]. Additionally, *SGK1*, encoding Serum and Glucocorticoid-regulated Kinase-1, was significantly downregulated. *SGK1* was identified as a target of an intergenic region harboring the rs4896104 SNP (**Fig. 4d**). This serine-threonine kinase regulates SCN5A activity and has been implicated as a therapeutic target for cardiac arrhythmias[39,40]. These findings suggest epistatic interactions in multiple genomic regions regulating distinct and overlapping pathways may culminate in AF .

EP Alterations in LMNA-S143P iPSC-aCMs

To assess the electrophysiological (EP) profile of *LMNA*-S143P iPSC-aCMs[41,42,43], we measured evoked action potentials (AP) in isolated mature iPSC-aCMs. *LMNA*-S143P iPSC-aCMs exhibited altered AP profiles, including reduced AP amplitude and upstroke velocity (dV/dTmax), a key indicator of atrial conduction, while AP duration at 90% repolarization (APD90) remained unchanged (**Fig. 5a-d**). AP amplitude and upstroke velocity are primarily determined by the peak I_{Na}, conducted via the main cardiac sodium channel Nav1.5, encoded by *SCN5A*. Consistently, voltage-clamp recordings revealed a significant reduction in peak I_{Na} density in *LMNA*-S143P iPSC-

aCMs compared to WT and *LMNA*-S143P-CRISPR-corrected cells (**Fig. 5e-f**). Stimulated multielectrode array recordings further demonstrated marked conduction heterogeneity across *LMNA*-S143P iPSC-aCM monolayers, a pattern absent in WT and corrected iPSCs (**Fig. 5g**). Importantly, potassium (I_K) and calcium (I_{Ca}) currents, which regulate the repolarization phase of the AP, remained unchanged, reinforcing that the observed EP changes in *LMNA*-S143P iPSC-aCMs are primarily driven by alterations in I_{Na} (**Supplementary Fig. 7**). In summary, reduced conduction velocity due to *SCN5A* downregulation in *LMNA*-S143P iPSC-aCMs promotes re-entry, establishing an arrhythmogenic substrate for early-onset AF.

Altered Calcium Handling and contractility in LMNA-S143P iPSC-aCMs

Calcium transient measurements revealed that *LMNA*-S143P iPSC-aCMs exhibited reduced transient amplitude and duration and irregular transient intervals **(Fig. 6a-d)**. Contractility assessments further demonstrated a decrease in contractile amplitude in *LMNA*-S143P iPSC-aCMs compared to controls (**Fig. 6f**). Transmission electron microscopy identified key myopathic features, including nuclear deformities, myofibrillar disarray and disrupted intercalated discs, consistent with histopathological findings in Lamin A/C cardiomyopathy [44](**Fig. 6g-i**). Collectively, these disruptions in calcium handling and contractility support the electromechanical dysfunction underlying atrial myopathy and AF[45].

CRISPR activation of SCN5A restores sodium current density in LMNA-S143P iPSC-aCMs

Electrophysiological analysis suggested that reduced I_{Na} in *LMNA*-S143P iPSC-aCMs may result from a closed chromatin conformation at the *SCN5A-SCN10A* locus. We employed a nuclease-deficient Cas9 (dCas9) fused to transcriptional activators

Vp64, p65, and Rta to upregulate SCN5A transcription to test this hypothesis. For the *SCN10A* enhancer region, we utilized a specific transcriptional activator, p300, which possesses histone acetyltransferase activity, facilitating chromatin remodeling and enhancer activation[46]. Transfection of both CRISPR activation complexes successfully restored *SCN5A* expression and I_{Na} in *LMNA*-S143P iPSC-aCMs, supporting our hypothesis that reduced chromatin accessibility at this locus contributes to I_{Na} deficiency (**Fig. 7a-e**). These findings establish a genomic mechanism underlying a pro-fibrillatory, re-entrant substrate driven by reduced I_{Na}.

Risk of Incident AF in carriers of LMNA protein-altering variants according to PRS

To assess the contribution of common variants to the variable penetrance of early-onset AF in Lamin A/C cardiomyopathy[8] we applied a PRS for AF to carriers of PAVs, including missense, frameshift, stop-gain, splice, and in-frame insertion variants in *LMNA*, using data from the UK Biobank and *All of Us* (AoU) cohorts. In the UK Biobank, we identified 1,109 carriers of 296 distinct rare *LMNA* PAVs, with an age distribution ranging from 40 to 70 years (median 58 [Q1-Q3: 50-64]), of whom 613 were female. AF prevalence was higher among *LMNA* PAV carriers (n = 89, 8.03%) compared to non-*LMNA* carriers (n = 20,917, 4.99%) ($p = 5.08 \times 10^{-6}$). In non-*LMNA* carriers, a high PRS was significantly associated with an increased risk of AF (hazard ratio [HR] 4.11, $p < 2 \times 10^{-16}$) (**Supplementary Fig. 9a, Supplementary Table 2**). However, the presence of rare *LMNA* PAVs conferred a two-fold increased risk of AF (HR 7.18, $p < 5.15 \times 10^{-5}$), after adjusting for the first 10 genetic principal components, sex, and hypertension (**Fig. 8a**, **Supplementary Table 3**).

We evaluated the association between *LMNA* variants and AF using logistic regression, adjusting for the first 10 genetic principal components, sex, age at

recruitment, and hypertension in individuals under 65. *LMNA* variant carriers had significantly higher odds of AF (odds ratio [OR] 1.57, 95% confidence interval [CI] 1.12–2.11, $p < 4.33 \times 10^{-3}$) compared to non-*LMNA* carriers. The odds increased substantially to 8.17 (CI 2.29–29.2, $p < 1.23 \times 10^{-3}$) in *LMNA* carriers with a high AF PRS compared to those with a low PRS. In a time-to-event analysis, the cumulative risk of AF was significantly higher in younger *LMNA* carriers than in non-carriers (hazard ratio [HR] 1.56, $p = 3.01 \times 10^{-3}$) **(Supplementary Table 4)**. High PRS further amplified AF risk, with *LMNA* carriers exhibiting a nearly two-fold greater risk (HR 9.31, $p < 4.73 \times 10^{-4}$) compared to non-*LMNA* carriers (HR 4.4, $p < 2 \times 10^{-16}$) in the UK Biobank (**Fig. 8b and Supplementary Fig. 9b &10, Supplementary Tables 5-6**).

We further analyzed 37 carriers of *LMNA* variants classified as pathogenic/likely pathogenic (P/LP) for DCM in ClinVar, of whom six had AF. Four of these six individuals had a high-risk AF PRS (**Supplementary Table 7**). Notably, only one carrier with a P/LP variant had DCM, and this individual also had a high-risk AF PRS. However, due to the limited sample size of P/LP *LMNA* carriers, we could not calculate precise risk estimates for this group.

In the AoU database, we identified 2,511 carriers of *LMNA* PAVs, with an age range spanning 19 to 102 years (median age: 57). AF prevalence was higher among *LMNA* PAV carriers (7.9%) compared to non-*LMNA* carriers (6.18%). Additionally, *LMNA* PAV carriers had significantly increased odds of AF (OR 1.31, 95% CI 1.21–1.51, $p < 5.38 \times 10^{-4}$) relative to non-carriers. Stratification by AF PRS revealed that *LMNA* carriers in the high PRS group had significantly greater odds of AF than those in the low PRS group (OR 3.39, 95% CI 2.10–5.48, $p < 1.07 \times 10^{-7}$). Time-to-event analysis using Cox Proportional Hazards modeling, adjusted for the first 10 genetic principal components, sex, and race, further confirmed that a high PRS was associated with an elevated risk of AF (HR 1.18, $p = 0.000392$) (**Fig. 8c**).

To further investigate, we analyzed a subset of 510 *LMNA* PAV carriers with P/LP variants annotated in ClinVar, of whom 54 had AF. Within this P/LP carrier group, individuals with a high PRS had higher odds of AF than those with a low PRS (OR 2.7, 95% CI 1.02–7.42, $p = 0.06$). Consistently, time-to-event analysis confirmed that a high PRS was associated with an elevated risk of AF in this subset as well (HR 1.20, $p = 0.007$) (**Fig. 8d**).

Discussion

Large-scale exome-wide genetic studies have linked rare *LMNA* variants to early-onset AF[3]; however, the phenotypic expression and severity of AF among carriers remain highly variable. While pathogenic *LMNA* variants associated with DCM exhibit high penetrance, the final clinical phenotype is influenced by the combined effects of multiple variants of a range of effect sizes, contributing to the heritability of complex diseases like AF. Although a PRS quantifies the cumulative impact of common variants, it does not fully capture epistatic interactions, which may be non-additive and context-dependent[47-49].

By integrating gene expression, chromatin accessibility, and PC-Hi-C genomic interactions, we identified dysregulated regulatory networks in key AF susceptibility genes and regions harboring AF-associated SNPs. These findings reveal a novel molecular mechanism by which rare and common variant epistatic interactions contribute to arrhythmia pathogenesis. Specifically, we observed chromatin accessibility changes at AF-associated loci, including a variant-sensitive *SCN5A* enhancer. These alterations reduced *SCN5A* expression, diminished I_{Na}, and conduction abnormalities, creating a substrate for re-entrant AF.

To assess the clinical impact of these interactions, we applied an AF PRS in two large population cohorts, the UK Biobank and AoU. Carriers of rare *LMNA* variants

with a high PRS had a two-fold increased risk of early-onset AF compared to those with a lower PRS, particularly in individuals under 65. While prior studies suggest that common variants influence the penetrance of rare monogenic variants, our findings provide direct molecular evidence supporting an interaction effect [4,6].

Although multiple arrhythmogenic mechanisms are implicated in Lamin A/C cardiomyopathy, such as fibrosis, and gap junction remodeling, we did not find differential changes in regulatory interactions for genes involved in these processes. However, the reduced I_{Na} and observed genomic alterations at the *SCN5A-SCN10A* locus strongly suggest that common polymorphisms at this locus increase the genetic predisposition for early-onset AF.

Most AF risk loci identified through GWAS reside in non-coding regions with regulatory roles in gene expression. We observed altered chromatin accessibility at several AF-associated loci and their target genes. While a SNP within the *SCN10A* intronic region had the strongest effect, we also identified associations with *SGK1*, a kinase regulating ion channel activity; *NPTN*, a structural gene involved in atrial differentiation and heart rate regulation; and *CEP68*, which contributes to centrosome cohesion and is linked to sinus node dysfunction[37,38,40]. Although *SCN5A* downregulation emerged as the primary driver of arrhythmic risk, our findings suggest that AF results from broader disruptions involving ion and non-ion channel proteins, including regulatory enzymes and structural components.

To establish a causal link between chromatin remodeling and AF risk, we employed CRISPR activation to restore chromatin accessibility at the variant-sensitive *SCN5A-SCN10A* locus, a region strongly associated with AF and electrocardiographic traits[14,26,50]. This intervention successfully rescued sodium channel expression, demonstrating that interactions between common polymorphisms and sodium channel dysfunction contribute to early-onset AF in *LMNA* variant carriers. Sodium channel

dysfunction in individuals with *LMNA* variants has been previously reported in patients exhibiting type I Brugada-like EKG patterns following cardiac arrest, a condition commonly associated with impaired sodium channel activity[51]. Our study provides a mechanistic explanation for this association and supports the inclusion of *LMNA* in genetic testing panels for Brugada syndrome.

Several limitations of this study warrant consideration. While human cardiac tissue represents the ideal model for investigating AF pathophysiology, its limited availability necessitates using iPSC-aCMs as an alternative[52,53]. A recognized limitation of iPSC-derived models is their relative immaturity. To address this, we implemented a comprehensive maturation protocol that combines electrical and biochemical stimuli to mimic fetal and postnatal development[41]. This approach improved the structural and metabolic maturity of iPSC-aCMs, as demonstrated in our previous work modeling an *NPPA* variant, where we identified mitochondrial dysfunction and ion channel remodeling[41]. Compared to animal models, which exhibit species-specific differences in ion channel expression, iPSC-aCMs more accurately recapitulate the diversity of human atrial ion channels. Additionally, iPSC-aCMs offer a unique advantage by allowing the study of pathogenic mechanisms within a patient's genetic background, providing insights that other experimental models may not fully capture, particularly in assessing the cumulative effects of multiple common polymorphisms. Another limitation of this study is that our exploration of epistatic interactions was based on iPSC-aCMs derived from a single proband. While this approach provides functional evidence for how common variants modulate the variable expressivity of early-onset AF in *LMNA* variant carriers, future studies incorporating additional AF-linked rare variants will be essential to generalize these findings and further elucidate epistatic mechanisms.

The findings of this study have several important implications. While ion channel dysfunction plays a central role in arrhythmia pathogenesis, our results highlight the significance of chromatin remodeling at multiple AF-associated loci. This underscores the complex etiology of AF and the need to expand therapeutic strategies beyond traditional ion channel-targeting drugs. The interaction between a structural gene variant and an AF susceptibility locus enriched with variants associated with electrocardiographic traits establishes a direct link between atrial myopathy and AF. This suggests that screening for atrial myopathy, particularly in family members of affected individuals, may have prognostic value, especially in deciding which patients to select for anticoagulation therapy[10]. Additionally, our successful CRISPR-based activation of the *SCN5A-SCN10A* region demonstrates the potential of epigenetic modifiers as targeted therapeutic interventions for AF, particularly in *LMNA* variant carriers. Finally, our findings highlight the necessity for improved genetic risk prediction models for AF and other complex diseases. Such models should integrate the cumulative effects of common variants with small effect sizes alongside highly penetrant rare variants while accounting for epistatic interactions.

Methods

Recruitment of participants

We used the UIC Institutional Review Board–approved protocol to enroll participants after receiving informed written consent.

Generation of human iPSCs and differentiation to atrial cardiomyocytes iPSC-aCMs

Human iPSCs were derived from reprogrammed peripheral blood mononuclear cells (PBMCs) from the proband and unaffected controls, as previously described[54]. iPSCs were differentiated using the STEMdiff atrial cardiomyocyte differentiation kit. The atrial cardiomyocyte population was purified through glucose starvation and lactate replacement, resulting in contracting monolayers of iPSC-aCMs. Human iPSC-aCMs were then matured using the maturation protocol following dissociation and replating on fibronectin-coated plates and maintained in Cardiomyocyte Maintenance Media supplemented with T3, insulin-like growth factor-1, and dexamethasone as previously described[41,43]. Our protocol typically yields ~80 to 90% pure iPSC-aCMs and fibroblasts based on immunostaining analysis, as we have previously described[41,43,54].

Generation of isogenic control from LMNA-S143P by CRISPR correction

As previously described, the isogenic control (LMNA-S143P Corrected) was generated using the Alt-R CRISPR-Cas9, homology-directed repair (HDR) system. [41]. Single guide (sg)RNAs and HDR oligos were nucleofected in *LMNA*-S143P hiPSCs. The sgRNAs were designed using the IDT CRISPR design tool based on an algorithm predicting optimal off-target and on-target scores. sgRNA 5'GGAGGCTCTGCTGAACCCCA-3' was used for genetic correction of Pro143 to Ser,

C to T in exon 2. Single-cell clones were isolated, expanded, and verified by next-generation sequencing and Sanger sequencing **(Supplementary Fig. 3b)**.

Electrophysiology

Whole-cell -patch-clamp recordings on single-cell iPSC-aCMs to measure INa, ICa, L, and IK were performed according to previously published protocols using the Axopatch 200B amplifier controlled by pClamp10 software through an Axon Digidata 1440A[41,43,54]. Sodium current measurements were done in a voltage clamp setup; pipettes were filled in mM: 135 CsF, 5 NaCl,5 MgATP, 10 Hepes, 10 EGTA, pH 7.2 with CsOH. Cells were perfused with a solution in mM: 85 CsCl, 10 glucose, 1 MgCl2, 1 CaCl2, 20 Hepes, 50 NaCl, pH 7.4 with CsOH.; 10 uM Nifedipine was added to block calcium channel. Sodium current was elicited by a series of 600 ms test potentials varying from -90 to -50 mV in 5 mV increments from a holding potential of -120 mV.

L-type calcium current was obtained in the whole cell voltage clamp configuration. External recording solution contained (in mM) 136 TEA-Cl, 2 CaCl2, 1.8 MgCl2, 10 HEPES, 5 4-aminopyridine, and 10 glucose (pH 7.4 with TEA-OH). The pipette solution contained (in mM): 125 CsCl, 20- TEA-Cl, 10 EGTA, 10 HEPES, 5 phosphocreatine, 5 Mg2ATP (pH 7.2 with CsOH). IPSC-aCM were held at -80 mV, and 10 mV depolarizing steps from -50 mV to + 50 mV for 300 ms were applied. Recording solutions allowed for the specific measurement of the calcium current without the contaminating Na and K currents.

Potassium current was measured in a whole cell rupture voltage clamp with patch clamp pipettes filled with internal solution in mM: 100 K-aspartate, 20 KCl, 5 Mg ATP, 2 MgCl2, 10 HEPES, 5 EGTA pH 7.2 with KOH; External solution was normal tyrode solution in mM: 140 NaCl, 4 KCl, 1.2 MgCl2, 1.8 CaCl2, 10 glucose, 10 HEPES pH

7.4 with NaOH; 10 uM Nifedipine was added to block calcium channels. IK outward current was measured from a holding potential of -60 mV to test potentials of –30 mV to +50 mV with 20 mV increments for 3 seconds.

Calcium transient recordings and Contractility Measurements

The Ionoptix system was used for contractility and calcium transient measurements. Contracting monolayers of iPSC-aCMs were incubated in 1uM Fura 2 AM calcium binding dye dissolved in Tyrode's solution. After 20 min of incubation, the dye solution was removed and replaced with Tyrode's solution. Calcium transients were analyzed using the ION-OPTIX analysis software. The software performs background detection and generates traces after subtraction of the background. Cytomotion, a label-free detection system, was used for contractility analysis, which provides high-speed data acquisition at 1000Hz. Differences in contractile amplitude measured inotropic differences. Contractility and calcium transient analysis by the ION wizard software is done according to an algorithm optimized for iPSC-derived cardiomyocytes.

Conduction Velocity Recordings

iPSC-aCMs from the three groups were plated on dishes with multi-electrode arrays. Biphasic stimuli were applied to iPSC-aCMs at an amplitude of 1000mV for a duration of 800us for 15 cycles. CV across the arrays was measured using the Cardio 2D software at each stimulus. Conduction velocities were generated from the software based on the time of stimulus application to measure electrical impulse across the array.

CRISPR activation

Tracr RNAs targeting the *SCN5A* promoter and *SCN10A* intronic enhancer were cloned into backbones with sgRNA scaffold (addgene#47108). iPSC-aCMs were co-

transfected with individual plasmids with sgRNAs, dCas9- VP64-p65-Rta (addgene#63798) or dCas9 CBP/ p300(addgene # 61357) and a plasmid with a GFP expression cassette (addgene#40973). dCas9- VP64-p65-Rta was used for activation of SCN5A promoter while dCas9 CBP/ p300 was used for SCN10A enhancer activation. All transfections were done using Lipofectamine 3000 according to the manufacturer's protocol. 48 hrs post-transfection, GFP-positive iPSC-aCMs were selected for sodium current measurements.

SCN5A sgRNA sequences	***PAM***
AGCGGGCGGAGCACCACGTG	***CGG***
AGCCCCAGGCCGAACCCAGG	***CGG***
gGACAGACAGACATAGGCGG	***GGG***
gTGAGCCCCCGGGTCAGTGT	***GGG***

SCN10A sgRNA sequences	***PAM***
TGTCCAGAGGTCAAAATTGT	***AGG***
TAACTGAAAATGCTTCTGAG	***TGG***
CTCTGCTGTTACCTAGACAA	***AGG***
GGAACACAAGTGACGACTGC	***AGG***

RNA sequencing, ATAC sequencing, and Bioinformatic Analysis

RNA extraction and library preparation on triplicate samples of ~ 1 million cells was done by the University of Chicago genome sequencing core. RNA was isolated using

Trizol and QC-ed by bioAnalyzer (Agilent 2100); RNA-seq libraries were generated using an Illumina TruSEQ-like protocol (provided by Illumina). Libraries were QC-ed by BioAnalyzer and sequenced on the Illumina NovaSEQ-X using reagents and protocols provided by Illumina. Raw FASTQ files were uploaded to Biojupies (https://maayanlab.cloud/biojupies) for analysis. Gene enrichment analysis was performed using ShinyGO 0.81 and Ingenuity Pathway Analysis (IPA). IPA was also used for upstream regulator and transcription factor analysis.

For ATAC-seq, Triplicate samples of ~ 500K single dissociated live iPSC-aCMs were provided to the Genomic Sequencing Core at Northwestern University for Library preparation. Briefly, the Cell membrane was permeabilized with nuclear lysis buffer (10 mM tris, 10 mM NaCl, 3 mM MgCl2, and 0.5% IGEPAL-630). Then, cells were resuspended in 50uL of transposase reaction mixture (22.5uL nuclease-free water, 25uL of TD buffer, and 2.5uL of TDE1 enzyme, Illumina #20034197). Transposition was carried out at 37°C for 22 min, followed by DNA purification with DNA Clean and Concentrator-5 (Zymo Research) according to the manufacturer's recommendation. Following purification, library fragments were PCR amplified with Nextera XT v2 adapter primers. Multiplexed and pooled library was sequenced on the Novaseq X Plus with paired ends of 50 nucleotides per the manufacturer's instructions. The library preparation and sequencing were done at the Northwestern University NUSeq facility core. The raw data was analyzed by the University of Illinois research informatics core.

ATAC-seq Analysis

Peak calling

Read alignments were first adjusted to account for TAC transposon binding: +4 bp for + strand alignments, -5 bp for - strand alignments. The open chromatin enrichment track was generated by first creating a bedGraph from the raw reads using bedtools

genomcov[55], then converted to bigWig using the UCSC tool bedGraphToBigWig [56]. Tracks were normalized by the sum of alignment lengths of over 1 billion. The start position track was generated by taking just the first base of the alignment for + strand alignments or the last base of the alignment for - strand alignments, then creating bedGraph and bigWig tracks as for the open chromatin; tracks were normalized to the alignment count over 1 million. Open chromatin peaks were called using MACS2[57] with --nomodel set and no background provided; peaks with a score >5 were retained.

Differential analysis of detected peaks

Differential analysis of quantitated peaks compared to genotype was performed using the software package edgeR on raw peak counts[58] Before analysis, the data were filtered to remove any peaks that had less than 20 total counts summed across all samples. Data were normalized as counts per million, and an additional normalization factor was computed using the TMM algorithm. Statistical tests were performed using the “exactTest” function in edgeR. Adjusted p values (q values) were calculated using the Benjamini-Hochberg false discovery rate (FDR) correction[59].Significantly enriched peaks were determined based on an FDR threshold of 5% (0.05).

RT-PCR

Total RNA was isolated from iPSC-aCMs using a Qiagen RNA extraction kit. Reverse transcription to synthesize cDNA was conducted using SuperScript III Reverse Transcriptase (Thermo Fisher Scientific). For the qPCR analysis, specific assays and primers were selected for target genes with glyceraldehyde 3-phosphate dehydrogenase (GAPDH) as the normalization reference gene. qPCR reactions were performed on an ABI QuantStudio 5 system (Applied Biosystems), using SYBR Green PCR Master Mix to accurately detect and quantify PCR amplification products.

Relative expression levels of the target genes were calculated using the ΔΔCt method by quantifying gene expression changes in the experimental samples relative to the control. For the ΔCt calculation, the cycling time (Ct) value of the target gene was subtracted from the Ct value of GAPDH in the same sample using $\Delta Ct = Ct_{target\ gene} - Ct_{reference\ gene}$. The ΔΔCt value was then calculated using $\Delta\Delta Ct = \Delta Ct_{experimental} - \Delta CT_{control}$. The gene's relative expression was calculated using relative gene expression = $2^{-\Delta\Delta Ct}$. **Primer pair for *SCN5A*- Forward- TCTCTATGGCAATCCACCCCA, Reverse- GAGGACATACAAGGCGTTGGT**

Western Blotting

Protein lysates from iPSC-aCMs were isolated using 1× RIPA buffer. Based on previously published protocols. Each sample containing 50 μg of protein was subjected to SDS-PAGE gel electrophoresis. The resolved gels were then electro-transferred onto 0.2 μm PVDF membranes. After a 2-hour blocking step with 5% BSA, membranes were probed with specific antibodies for target proteins (Supplemental Table 3). Blots were developed using either anti-rabbit HRP or anti-mouse HRP and scanned with C280 imaging systems (Azure Biosystems). ImageJ software was used to determine protein expression levels. Antibody used for SCN5A- **68273-1-Ig SCN5A Mouse McAb from protein tech.**

Immunofluorescence

iPSC-aCMs were washed with PBS, fixed with 4% paraformaldehyde at 37°C for 10 minutes, 0.1% Triton X-100 was used for permeabilization for 15 minutes, and blocked with 10% BSA for 1 hour. Primary antibody was diluted at 1:200 in 10% BSA and incubated in 10% BSA at 4°C overnight. The secondary antibody was incubated in 1:1000 dilution in 10% BSA for 1 hour. Primary antibodies utilized were rabbit polyclonal anti-cTnT (Abcam; ab45932) and mouse anti-sarcomeric anti–α-actinin

(Abcam; EA-53 ab9465). Secondary antibodies used were goat anti-rabbit Alexa Fluor 488 (Abcam; ab150077) and goat anti-mouse Alexa Fluor 594 (Abcam; 150116). Nuclei were stained using DAPI (Thermo Fisher Scientific). The cells were visualized using a Zeiss Laser Scanning confocal microscope (LSM 710) (META) objective and analyzed on ImageJ (NIH).

Transmission Electron Microscopy

hiPSC-aCMs were fixed in Warmed (37°C) 2.5% glutaraldehyde in 0.1 M Sorenson's Buffer for 60 min at room temperature, followed by gently scraping cells into a microcentrifuge tube prefilled with 2.5% glutaraldehyde in 0.1 M Sorenson's buffer. Samples were centrifuged at 2500 g for 10 min at room temperature, and the pellet was dislodged and flipped with a hypodermic needle to ensure the fixative solution penetrated the entire sample. The pellet was kept at room temperature to fix for an additional 60 min. The 2.5% glutaraldehyde in 0.1 M Sorenson's buffer solution was removed and replaced with 1% glutaraldehyde +4% paraformaldehyde in 0.1 M Sorenson's buffer and stored at 4°C.

Data Analysis and Statistics

All experiments were done in a minimum of three groups and repeated across at least three independent differentiations. Data was presented as mean ± SD. For data with normal distribution, nonparametric unpaired and 2-tailed Mann-Whitney U test was used to determine statistical significance between 2 groups and either 1-way or 2-way ANOVA for multiple groups with post hoc Bonferroni's corrections. $P < 0.05$ was considered significant.

UK Biobank and AoU PRS methods

The UK Biobank standard AF PRS (data field 26212) derived by Genomics PLC from external data sources was used[60,61]. The UK Biobank recruited over 500,000 participants aged 40 to 69 years old between 2006 and 2010 from multiple centers across the United Kingdom[62]. Ethics approval was obtained from National Research Ethics Service (reference 11/NW/0382). All participants provided written informed consent. Analyses were performed on the UK Biobank research analysis platform (application number 47602). The PRS for 420,196 participants was classified into 3 categories of genetic risk (low-risk [bottom quintile], high-risk [top quintile] and medium-risk [middle quintiles]. Logistic regression was used to assess the association of AF with PRS. Cox regression was used to calculate the hazard ratio (HR) for AF across PRS categories adjusting for the first 10 genetic PCs, sex, age and hypertension. Time to AF diagnosis (date at first diagnosis, data field 131350) was visualized with Kaplan Meier curves.

AoU Controlled Tier Dataset, version 7 was utilized in this study. AF cases were identified using OMOP Concept IDs: 313217, 321319, 3656119, 4064452, 4071896, 4108822, 4108832, 4117112, 4124693, 4141360, 4154290, 4163710, 4178584, 4199501, 4232495, 4232691, 4232697, 42872390, 44782442, 44783568, and 45768480. Whole-genome sequencing data from AoU were extracted and subjected to quality control using PLINK v1.9. This involved filtering out SNPs with a minor allele frequency (MAF) of < 0.01 and excluding SNPs with a genotyping rate < 95%.

SNP pruning was performed using PLINK with a 50 kb sliding window, shifted by 5 SNPs at each step, and an r^2 threshold of 0.2. The pruned SNPs were then used to compute genetic principal components (PCs) via PLINK. For Polygenic Risk Score (PRS) calculation, GWAS summary statistics for AF were obtained from a recent PRS analysis in individuals from the UK Biobank [63] , and genomic coordinates were lifted

over from hg19 to hg38 using the pyliftover tool (https://github.com/konstantint/pyliftover).

The PRS was classified into three categories of genetic risk: low-risk (bottom quintile), medium-risk (middle quintiles), and high-risk (top quintile). Survival analysis was conducted using Cox Proportional Hazards modeling, with age at diagnosis serving as the time-to-event variable.

References

1 Elliott, A. D., Middeldorp, M. E., Van Gelder, I. C., Albert, C. M. & Sanders, P. Epidemiology and modifiable risk factors for atrial fibrillation. *Nature Reviews Cardiology* **20**, 404-417 (2023). https://doi.org:10.1038/s41569-022-00820-8

2 Sweat, M. E. & Pu, W. T. Genetic and molecular underpinnings of atrial fibrillation. *npj Cardiovascular Health* **1**, 35 (2024). https://doi.org:10.1038/s44325-024-00035-5

3 Choi, S. H. *et al.* Sequencing in over 50,000 cases identifies coding and structural variation underlying atrial fibrillation risk. *Nature Genetics* (2025). https://doi.org:10.1038/s41588-025-02074-9

4 Vad, O. B. *et al.* Rare and Common Genetic Variation Underlying Atrial Fibrillation Risk. *JAMA Cardiol* **9**, 732-740 (2024). https://doi.org:10.1001/jamacardio.2024.1528

5 Marston, N. A. *et al.* A polygenic risk score predicts atrial fibrillation in cardiovascular disease. *European Heart Journal* **44**, 221-231 (2022). https://doi.org:10.1093/eurheartj/ehac460

6 Ritchie Marylyn, D. *et al.* Chromosome 4q25 Variants Are Genetic Modifiers of Rare Ion Channel Mutations Associated With Familial Atrial Fibrillation. *Journal of the American College of Cardiology* **60**, 1173-1181 (2012). https://doi.org:10.1016/j.jacc.2012.04.030

7 Chen, S. N., Sbaizero, O., Taylor, M. R. G. & Mestroni, L. Lamin A/C Cardiomyopathy: Implications for Treatment. *Curr Cardiol Rep* **21**, 160 (2019). https://doi.org:10.1007/s11886-019-1224-7

8 Tremblay-Gravel, M. *et al.* Intrinsic Atrial Myopathy Precedes Left Ventricular Dysfunction and Predicts Atrial Fibrillation in Lamin A/C Cardiomyopathy. *Circ Genom Precis Med* **16**, e003480 (2023). https://doi.org:10.1161/circgen.121.003480

9 Lazarte, J. *et al.* LMNA Variants and Risk of Adult-Onset Cardiac Disease. *J Am Coll Cardiol* **80**, 50-59 (2022). https://doi.org:10.1016/j.jacc.2022.04.035

10 Foreman, K. L., Shusta, E. V. & Palecek, S. P. Defined Differentiation of Human Pluripotent Stem Cells to Brain Microvascular Endothelial-Like Cells for Modeling the Blood-Brain Barrier. *Methods Mol Biol* **2683**, 113-133 (2023). https://doi.org:10.1007/978-1-0716-3287-1_10

11 Wang, Y. *et al.* Lamin A/C-dependent chromatin architecture safeguards naïve pluripotency to prevent aberrant cardiovascular cell fate and function. *Nature Communications* **13**, 6663 (2022). https://doi.org:10.1038/s41467-022-34366-7

12 Lavine, K. Genomic reorganization underlies LMNA-associated cardiomyopathies. *Science Translational Medicine* **11**, eaaw7627 (2019). https://doi.org:doi:10.1126/scitranslmed.aaw7627

13 Delafrouz, P., Farooq, H., Du, L., Ma, A. & Liang, J. Effects of Lamina-Chromatin Attachment on Super Long-Range Chromatin Interactions. *bioRxiv* (2025). https://doi.org:10.1101/2025.02.13.638183

14 van den Boogaard, M. *et al.* A common genetic variant within SCN10A modulates cardiac SCN5A expression. *J Clin Invest* **124**, 1844-1852 (2014). https://doi.org:10.1172/jci73140

15 Choi, S. H. *et al.* Association Between Titin Loss-of-Function Variants and Early-Onset Atrial Fibrillation. *Jama* **320**, 2354-2364 (2018). https://doi.org:10.1001/jama.2018.18179

16 Montefiori, L. E. *et al.* A promoter interaction map for cardiovascular disease genetics. *Elife* **7**, e35788 (2018). https://doi.org:10.7554/eLife.35788

17 https://www.ncbi.nlm.nih.gov/clinvar/variation/66899/.

18 Richards, S. *et al.* Standards and guidelines for the interpretation of sequence variants: a joint consensus recommendation of the American College of Medical Genetics and Genomics and the Association for Molecular Pathology. *Genet Med* **17**, 405-424 (2015). https://doi.org:10.1038/gim.2015.30

19 Shah, D. *et al.* Modeling of LMNA-Related Dilated Cardiomyopathy Using Human Induced Pluripotent Stem Cells. *Cells* **8** (2019). https://doi.org:10.3390/cells8060594

20 Kärkkäinen, S. *et al.* A novel mutation, Ser143Pro, in the lamin A/C gene is common in finnish patients with familial dilated cardiomyopathy. *Eur Heart J* **25**, 885-893 (2004). https://doi.org:10.1016/j.ehj.2004.01.020
21 Briand, N. & Collas, P. Lamina-associated domains: peripheral matters and internal affairs. *Genome Biology* **21**, 85 (2020). https://doi.org:10.1186/s13059-020-02003-5
22 van Steensel, B. & Belmont, A. S. Lamina-Associated Domains: Links with Chromosome Architecture, Heterochromatin, and Gene Repression. *Cell* **169**, 780-791 (2017). https://doi.org:10.1016/j.cell.2017.04.022
23 Olesen, M. S. *et al.* High prevalence of long QT syndrome-associated SCN5A variants in patients with early-onset lone atrial fibrillation. *Circ Cardiovasc Genet* **5**, 450-459 (2012). https://doi.org:10.1161/circgenetics.111.962597
24 Darbar, D. *et al.* Cardiac sodium channel (SCN5A) variants associated with atrial fibrillation. *Circulation* **117**, 1927-1935 (2008). https://doi.org:10.1161/circulationaha.107.757955
25 Yoneda, Z. T. *et al.* Early-Onset Atrial Fibrillation and the Prevalence of Rare Variants in Cardiomyopathy and Arrhythmia Genes. *JAMA Cardiol* **6**, 1371-1379 (2021). https://doi.org:10.1001/jamacardio.2021.3370
26 Miyazawa, K. *et al.* Cross-ancestry genome-wide analysis of atrial fibrillation unveils disease biology and enables cardioembolic risk prediction. *Nature Genetics* **55**, 187-197 (2023). https://doi.org:10.1038/s41588-022-01284-9
27 Maitra, M. *et al.* Interaction of Gata4 and Gata6 with Tbx5 is critical for normal cardiac development. *Dev Biol* **326**, 368-377 (2009). https://doi.org:10.1016/j.ydbio.2008.11.004
28 Broman, M. T. *et al.* A Genomic Link From Heart Failure to Atrial Fibrillation Risk: FOG2 Modulates a TBX5/GATA4-Dependent Atrial Gene Regulatory Network. *Circulation* **149**, 1205-1230 (2024). https://doi.org:10.1161/CIRCULATIONAHA.123.066804
29 Yang, Y.-Q. *et al.* GATA4 loss-of-function mutations in familial atrial fibrillation. *Clinica Chimica Acta* **412**, 1825-1830 (2011). https://doi.org:https://doi.org/10.1016/j.cca.2011.06.017
30 Maitra, M. *et al.* Interaction of Gata4 and Gata6 with Tbx5 is critical for normal cardiac development. *Developmental Biology* **326**, 368-377 (2009). https://doi.org:https://doi.org/10.1016/j.ydbio.2008.11.004
31 Sweat, M. E. *et al.* Tbx5 maintains atrial identity in post-natal cardiomyocytes by regulating an atrial-specific enhancer network. *Nat Cardiovasc Res* **2**, 881-898 (2023). https://doi.org:10.1038/s44161-023-00334-7
32 Laforest, B. *et al.* Atrial fibrillation risk loci interact to modulate Ca2+-dependent atrial rhythm homeostasis. *J Clin Invest* **129**, 4937-4950 (2019). https://doi.org:10.1172/jci124231
33 Arnolds, D. E. *et al.* TBX5 drives Scn5a expression to regulate cardiac conduction system function. *J Clin Invest* **122**, 2509-2518 (2012). https://doi.org:10.1172/jci62617
34 Roselli, C. *et al.* Multi-ethnic genome-wide association study for atrial fibrillation. *Nat Genet* **50**, 1225-1233 (2018). https://doi.org:10.1038/s41588-018-0133-9
35 Nielsen, J. B. *et al.* Biobank-driven genomic discovery yields new insight into atrial fibrillation biology. *Nat Genet* **50**, 1234-1239 (2018). https://doi.org:10.1038/s41588-018-0171-3
36 Weng, L.-C. *et al.* The impact of common and rare genetic variants on bradyarrhythmia development. *Nature Genetics* (2025). https://doi.org:10.1038/s41588-024-01978-2
37 Weng, L.-C. *et al.* The impact of common and rare genetic variants on bradyarrhythmia development. *Nature Genetics* **57**, 53-64 (2025). https://doi.org:10.1038/s41588-024-01978-2
38 Choy, M.-K., Liu, Y., Williams, S., Eales, J. & Keavney, B. BS13 Genome-wide association study coupled with promoter interactomic data identifies neuroplastin (NPTN) as a potential novel gene regulating heart rate. *Heart* **108**, A151-A152 (2022). https://doi.org:10.1136/heartjnl-2022-BCS.193

39 Bapat, A. *et al*. Genetic inhibition of serum glucocorticoid kinase 1 prevents obesity-related atrial fibrillation. *JCI Insight* **7** (2022). https://doi.org:10.1172/jci.insight.160885
40 Bezzerides, V. J. *et al*. Inhibition of serum and glucocorticoid regulated kinase-1 as novel therapy for cardiac arrhythmia disorders. *Sci Rep* **7**, 346 (2017). https://doi.org:10.1038/s41598-017-00413-3
41 Ly, O. T. *et al*. Mutant ANP induces mitochondrial and ion channel remodeling in a human iPSC-derived atrial fibrillation model. *JCI Insight* **7** (2022). https://doi.org:10.1172/jci.insight.155640
42 Brown, G. E. *et al*. Engineered cocultures of iPSC-derived atrial cardiomyocytes and atrial fibroblasts for modeling atrial fibrillation. *Sci Adv* **10**, eadg1222 (2024). https://doi.org:10.1126/sciadv.adg1222
43 Sridhar, A. *et al*. Modulation of NOX2 causes obesity-mediated atrial fibrillation. *J Clin Invest* **134** (2024). https://doi.org:10.1172/jci175447
44 Quarta, G. *et al*. Mutations in the Lamin A/C gene mimic arrhythmogenic right ventricular cardiomyopathy. *European Heart Journal* **33**, 1128-1136 (2011). https://doi.org:10.1093/eurheartj/ehr451
45 Lou, Q., Janardhan, A. & Efimov, I. R. Remodeling of calcium handling in human heart failure. *Adv Exp Med Biol* **740**, 1145-1174 (2012). https://doi.org:10.1007/978-94-007-2888-2_52
46 Hilton, I. B. *et al*. Epigenome editing by a CRISPR-Cas9-based acetyltransferase activates genes from promoters and enhancers. *Nature Biotechnology* **33**, 510-517 (2015). https://doi.org:10.1038/nbt.3199
47 Singhal, P. *et al*. Evidence of epistasis in regions of long-range linkage disequilibrium across five complex diseases in the UK Biobank and eMERGE datasets. *Am J Hum Genet* **110**, 575-591 (2023). https://doi.org:10.1016/j.ajhg.2023.03.007
48 Domingo, J., Baeza-Centurion, P. & Lehner, B. The Causes and Consequences of Genetic Interactions (Epistasis). *Annual Review of Genomics and Human Genetics* **20**, 433-460 (2019). https://doi.org:https://doi.org/10.1146/annurev-genom-083118-014857
49 Fiziev, P. P. *et al*. Rare penetrant mutations confer severe risk of common diseases. *Science* **380**, eabo1131 (2023). https://doi.org:doi:10.1126/science.abo1131
50 Butler, A. M. *et al*. Novel loci associated with PR interval in a genome-wide association study of 10 African American cohorts. *Circ Cardiovasc Genet* **5**, 639-646 (2012). https://doi.org:10.1161/circgenetics.112.963991
51 Armaroli, A. *et al*. Lamin A/C Missense Mutation R216C Pinpoints Overlapping Features Between Brugada Syndrome and Laminopathies. *Circulation: Genomic and Precision Medicine* **13**, e002751 (2020). https://doi.org:10.1161/CIRCGEN.119.002751
52 Ribeiro, A. J. S. *et al*. Considerations for an In Vitro, Cell-Based Testing Platform for Detection of Drug-Induced Inotropic Effects in Early Drug Development. Part 2: Designing and Fabricating Microsystems for Assaying Cardiac Contractility With Physiological Relevance Using Human iPSC-Cardiomyocytes. *Frontiers in Pharmacology* **10** (2019). https://doi.org:ARTN 934

10.3389/fphar.2019.00934
53 Liang, P. *et al*. Drug Screening Using a Library of Human Induced Pluripotent Stem Cell-Derived Cardiomyocytes Reveals Disease-Specific Patterns of Cardiotoxicity. *Circulation* **127**, 1677-+ (2013). https://doi.org:10.1161/Circulationaha.113.001883
54 Hong, L. *et al*. Human induced pluripotent stem cell-derived atrial cardiomyocytes carrying an SCN5A mutation identify nitric oxide signaling as a mediator of atrial fibrillation. *Stem cell reports* **16**, 1542-1554 (2021). https://doi.org:10.1016/j.stemcr.2021.04.019
55 Quinlan, A. R. & Hall, I. M. BEDTools: a flexible suite of utilities for comparing genomic features. *Bioinformatics* **26**, 841-842 (2010). https://doi.org:10.1093/bioinformatics/btq033

56 Kent, W. J., Zweig, A. S., Barber, G., Hinrichs, A. S. & Karolchik, D. BigWig and BigBed: enabling browsing of large distributed datasets. *Bioinformatics* **26**, 2204-2207 (2010). https://doi.org:10.1093/bioinformatics/btq351

57 Zhang, Y. *et al*. Model-based analysis of ChIP-Seq (MACS). *Genome Biol* **9**, R137 (2008). https://doi.org:10.1186/gb-2008-9-9-r137

58 McCarthy, D. J., Chen, Y. & Smyth, G. K. Differential expression analysis of multifactor RNA-Seq experiments with respect to biological variation. *Nucleic Acids Res* **40**, 4288-4297 (2012). https://doi.org:10.1093/nar/gks042

59 Zhang, Y. *et al*. Model-based Analysis of ChIP-Seq (MACS). *Genome Biology* **9**, R137 (2008). https://doi.org:10.1186/gb-2008-9-9-r137

60 Thompson, D. J. *et al*. UK Biobank release and systematic evaluation of optimised polygenic risk scores for 53 diseases and quantitative traits. *medRxiv*, 2022.2006.2016.22276246 (2022). https://doi.org:10.1101/2022.06.16.22276246

61 Thompson, D. J. *et al*. A systematic evaluation of the performance and properties of the UK Biobank Polygenic Risk Score (PRS) Release. *PLoS One* **19**, e0307270 (2024). https://doi.org:10.1371/journal.pone.0307270

62 Sudlow, C. *et al*. UK Biobank: An Open Access Resource for Identifying the Causes of a Wide Range of Complex Diseases of Middle and Old Age. *PLOS Medicine* **12**, e1001779 (2015). https://doi.org:10.1371/journal.pmed.1001779

63 Thompson, D. J. *et al*. UK Biobank release and systematic evaluation of optimised polygenic risk scores for 53 diseases and quantitative traits. *medRxiv*, 2022.2006.2016.22276246 (2022). https://doi.org:10.1101/2022.06.16.22276246

Table 1: Cardiac Phenotype of *LMNA*-S143P Kindred.

	AF	Conduction Disease	DCM	SCD	PPM/ICD	Additional Phenotyping
I-2			Yes			Died in '40s 5 out of 7 siblings died in the '40s due to CHF
II-2 +	Yes	Yes			PPM	
II-4		Yes	Yes		PPM	Heart transplant
II-5	Yes	Yes	Yes		CRT-D	
III-2 -						
III-3	Yes	Yes				Bradycardia, 1°AVB
III-4 +	Yes	Yes			BiV-PPM	Bradycardia, 1°AVB
III-7				Yes		
III-8						SVT, NSVT
III-9						POTS
III-5				Yes		Died in 30s'
III-6						SVT, NSVT
III-9						POTS

Abbreviations: congestive heart failure (CHF), biventricular pacemaker (BiV-PPM), atrioventricular block (AVB), supraventricular tachycardia (SVT), non-sustained ventricular tachycardia (NSVT), postural orthostatic tachycardia syndrome (POTS) "+" genotype positive, "-" genotype negative.

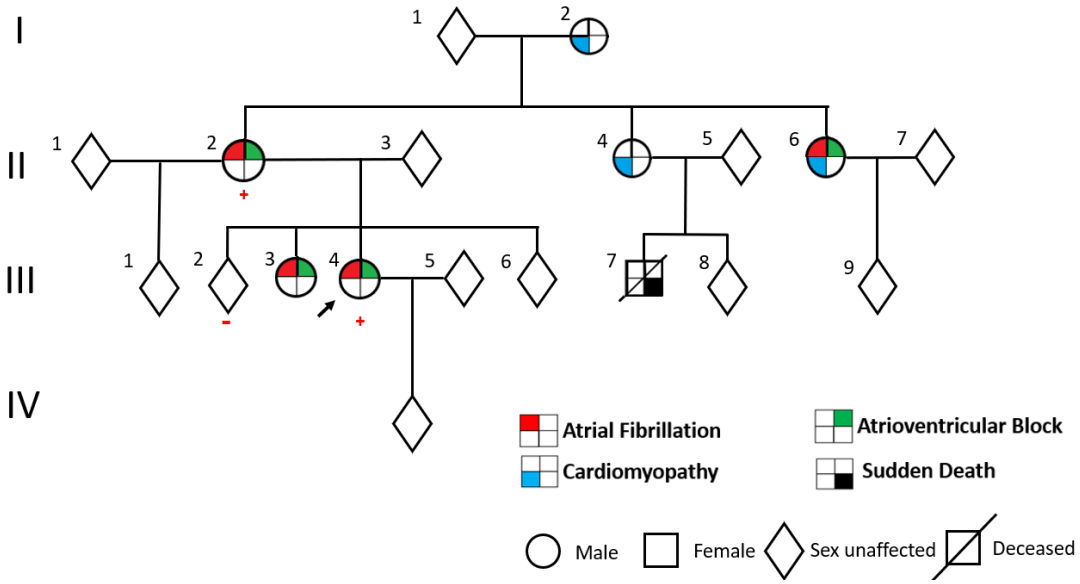
I
II
III
IV
Atrial Fibrillation
Cardiomyopathy
Atrioventricular Block
Sudden Death
Male
Female
Sex unaffected
Deceased

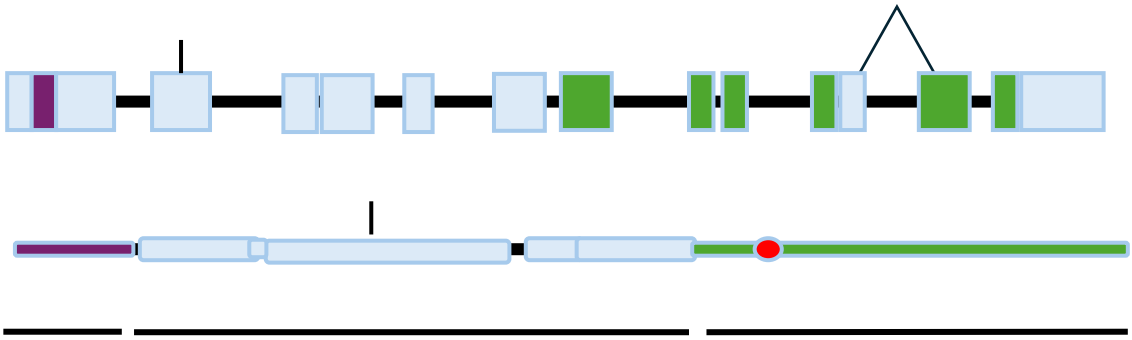

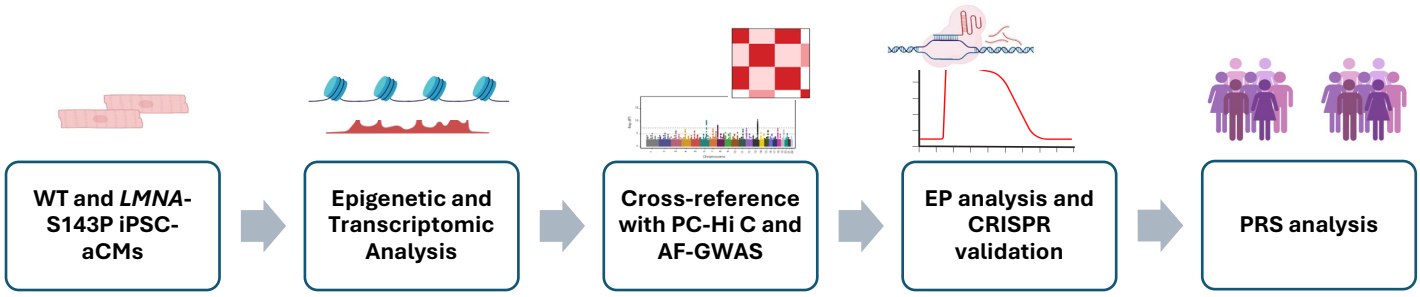
WT and *LMNA*-S143P iPSC-aCMs
Epigenetic and Transcriptomic Analysis
Cross-reference with PC-Hi C and AF-GWAS
EP analysis and CRISPR validation
PRS analysis

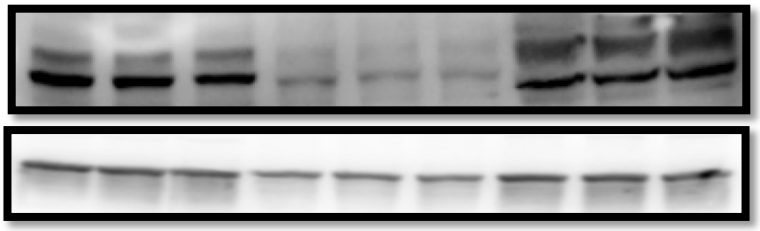

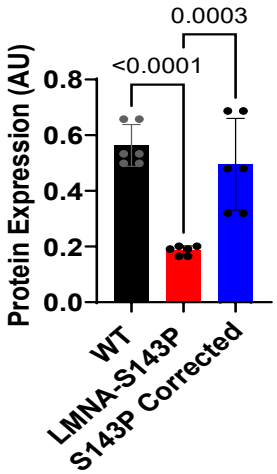
Protein Expression (AU)
0.8
0.6
0.4
0.2
0.0
<0.0001
0.0003
WT
LMNA-S143P
S143P Corrected

Fig. 1: Pedigree of a family harboring the pathogenic *LMNA*-S143P variant. a. Schematic representation of the family pedigree, highlighting affected members with a history of atrial fibrillation (AF), atrioventricular (AV) block, cardiomyopathy, and sudden death. The arrow indicates the proband. Circles denote females; squares denote males. The plus (+) and minus (-) signs indicate the presence and absence of the *LMNA*-S143P variant, respectively. **b.** Schematic illustrating the nucleotide and amino acid change (NM_170707.4(LMNA):c.427T>C [p.Ser143Pro]) in exon 2 and the central rod domain. The arrowhead marks an alternative splice site location for generating Lamin A and C transcripts. **c.** Overview of the study design. **d.** Protein expression analysis of Lamin A/C in wild-type (WT), LMNA-S143P, and S143P-corrected iPSC-aCMs.

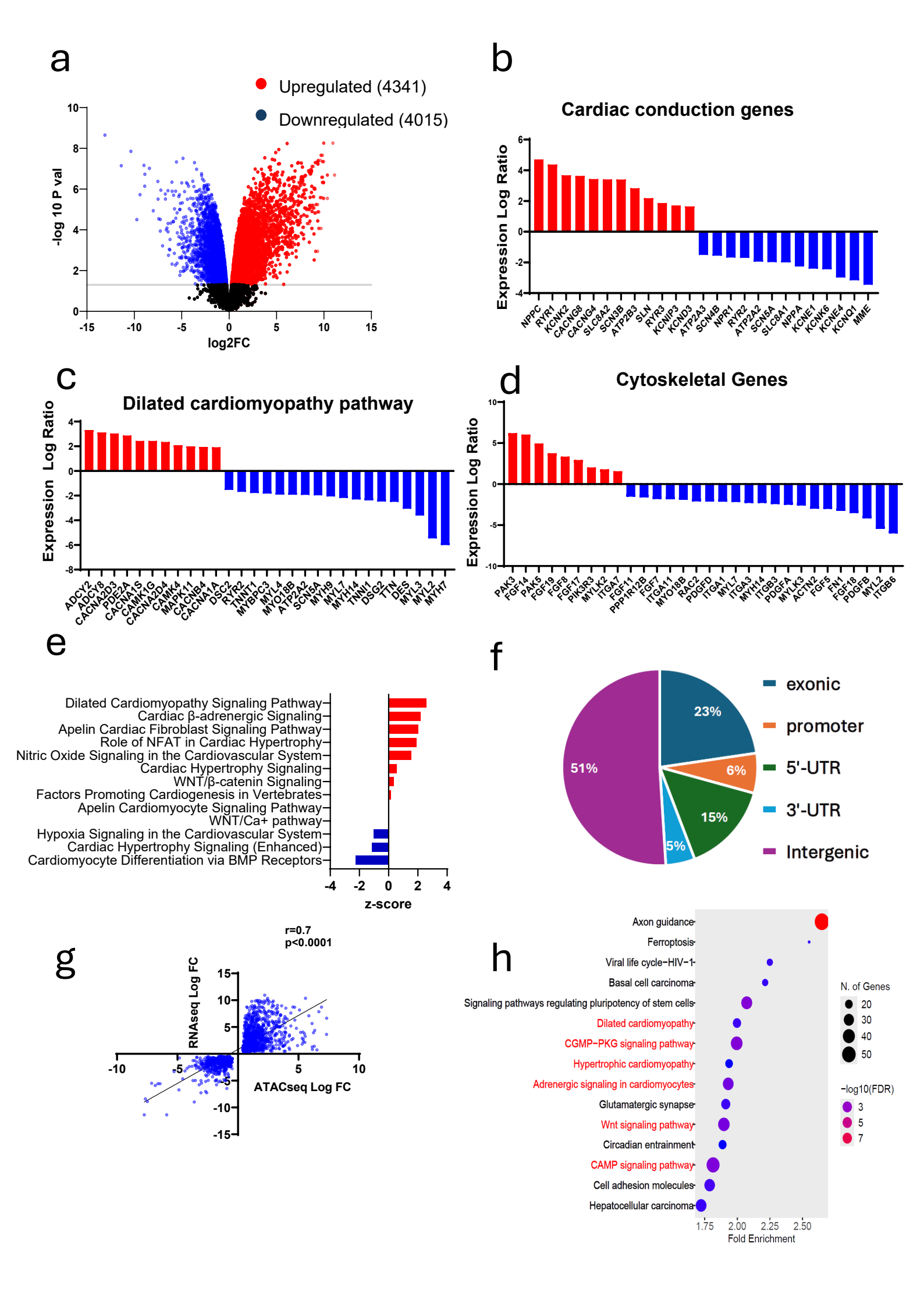
a
Upregulated (4341)
Downregulated (4015)
-log 10 P val
log2FC
b
Cardiac conduction genes
Expression Log Ratio
NPPC RYR1 KCNK2 CACNG8 CACNG4 SLC8A2 SCN3B ATP2B3 SLN RYR3 KCNIP3 KCND3 ATP2A3 SCN4B NPR1 RYR2 ATP2A2 SCN5A SLC8A1 NPPA KCNE1 KCNK6 KCNE4 KCNQ1 MME
c
Dilated cardiomyopathy pathway
Expression Log Ratio
ADCY2 ADCY8 CACNA2D3 PDE2A CACNA1S CAMK1G CACNA2D4 CAMK4 MAPK11 CACNB4 CACNA1A DSC2 RYR2 TNNT1 MYBPC3 MYL4 MYO18B ATP2A2 SCN5A MYH9 MYL7 MYH14 TNNI1 DSG2 TTN DES MYL3 MYL2 MYH7
d
Cytoskeletal Genes
Expression Log Ratio
PAK3 FGF14 PAK5 FGF19 FGF8 FGF17 PIK3R3 MYLK2 ITGA7 FGF11 PPP1R12B FGF7 ITGA11 MYO18B RAC2 PDGFD ITGA1 MYL7 ITGA3 MYH14 ITGB3 PDGFA MYLK3 ACTN2 FGF5 FN1 FGF18 PDGFB MYL2 ITGB6
e
Dilated Cardiomyopathy Signaling Pathway
Cardiac β-adrenergic Signaling
Apelin Cardiac Fibroblast Signaling Pathway
Role of NFAT in Cardiac Hypertrophy
Nitric Oxide Signaling in the Cardiovascular System
Cardiac Hypertrophy Signaling
WNT/β-catenin Signaling
Factors Promoting Cardiogenesis in Vertebrates
Apelin Cardiomyocyte Signaling Pathway
WNT/Ca+ pathway
Hypoxia Signaling in the Cardiovascular System
Cardiac Hypertrophy Signaling (Enhanced)
Cardiomyocyte Differentiation via BMP Receptors
z-score
f
exonic
promoter
5'-UTR
3'-UTR
Intergenic
23%
6%
15%
5%
51%
g
r=0.7
p<0.0001
RNAseq Log FC
ATACseq Log FC
h
Axon guidance
Ferroptosis
Viral life cycle−HIV−1
Basal cell carcinoma
Signaling pathways regulating pluripotency of stem cells
Dilated cardiomyopathy
CGMP−PKG signaling pathway
Hypertrophic cardiomyopathy
Adrenergic signaling in cardiomyocytes
Glutamatergic synapse
Wnt signaling pathway
Circadian entrainment
CAMP signaling pathway
Cell adhesion molecules
Hepatocellular carcinoma
N. of Genes
−log10(FDR)
Fold Enrichment

Fig. 2: Transcriptomic and chromatin accessibility changes in *LMNA-S143P* iPSC-aCMs. a. Volcano plot showing differentially expressed genes (DEGs) ($FDR < 0.05$, $log_2FC > 0$). **b-d.** Differential Gene expression changes in genes associated with dilated cardiomyopathy (DCM), cardiac conduction, and cytoskeletal function. **e.** Altered cardiovascular signaling pathways in *LMNA-S143P* iPSC-aCMs as identified through Ingenuity Pathway Analysis (IPA). **f.** Distribution of differential ATAC-seq peaks, illustrating that the majority are located in non-coding genomic regions. **g.** Positive correlation between gene expression and chromatin accessibility at promoters of differentially expressed genes. **h.** KEGG pathway analysis of differential ATAC peaks at promoter regions.

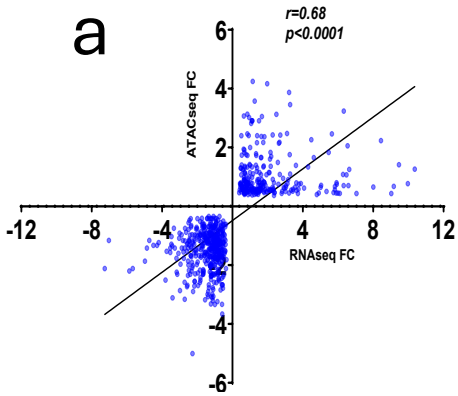
a
r=0.68
p<0.0001
ATACseq FC
RNAseq FC
6
4
2
-4
-6
-12
-8
-4
4
8
12

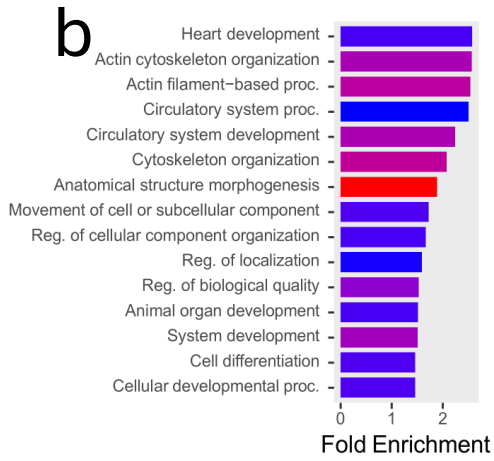
b
Heart development
Actin cytoskeleton organization
Actin filament−based proc.
Circulatory system proc.
Circulatory system development
Cytoskeleton organization
Anatomical structure morphogenesis
Movement of cell or subcellular component
Reg. of cellular component organization
Reg. of localization
Reg. of biological quality
Animal organ development
System development
Cell differentiation
Cellular developmental proc.
0
1
2
Fold Enrichment

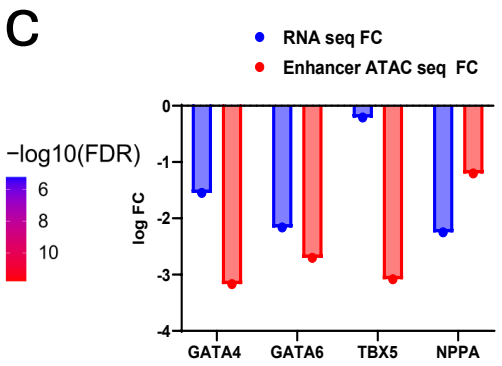
c
RNA seq FC
Enhancer ATAC seq FC
−log10(FDR)
6
8
10
log FC
0
-1
-2
-3
-4
GATA4
GATA6
TBX5
NPPA

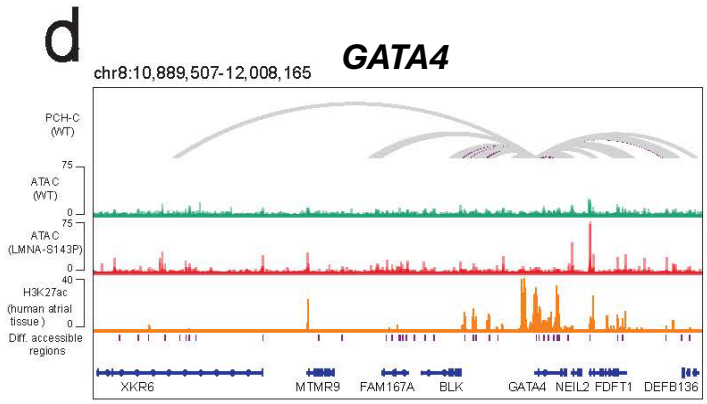
d
GATA4
chr8:10,889,507-12,008,165
PCH-C (WT)
ATAC (WT)
ATAC (LMNA-S143P)
H3K27ac (human atrial tissue)
Diff. accessible regions
XKR6
MTMR9
FAM167A
BLK
GATA4
NEIL2
FDFT1
DEFB136

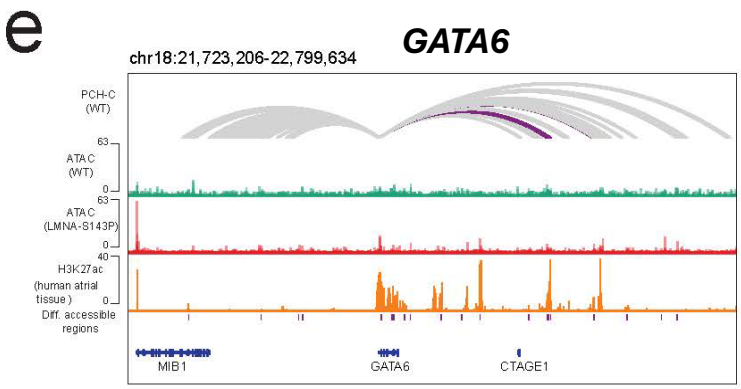
e
GATA6
chr18:21,723,206-22,799,634
PCH-C (WT)
ATAC (WT)
ATAC (LMNA-S143P)
H3K27ac (human atrial tissue)
Diff. accessible regions
MIB1
GATA6
CTAGE1

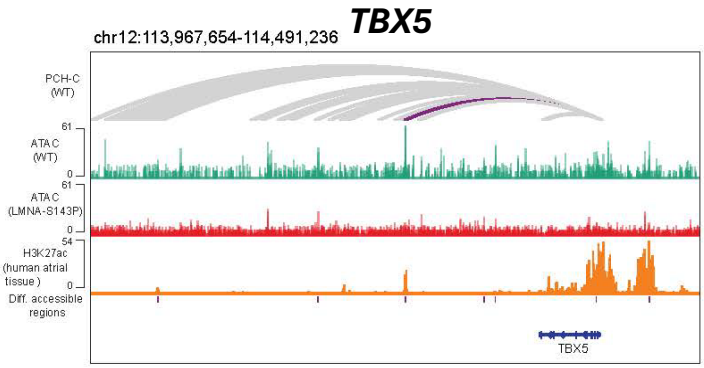
f
TBX5
chr12:113,967,654-114,491,236
PCH-C (WT)
ATAC (WT)
ATAC (LMNA-S143P)
H3K27ac (human atrial tissue)
Diff. accessible regions
TBX5

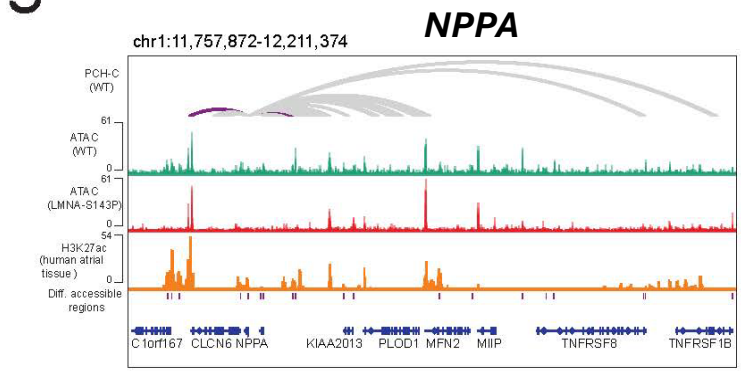
g
NPPA
chr1:11,757,872-12,211,374
PCH-C (WT)
ATAC (WT)
ATAC (LMNA-S143P)
H3K27ac (human atrial tissue)
Diff. accessible regions
C1orf167
CLCN6
NPPA
KIAA2013
PLOD1
MFN2
MIIP
TNFRSF8
TNFRSF1B

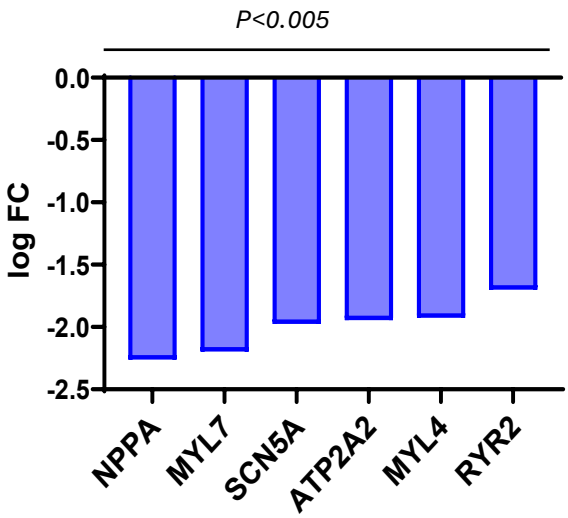
h
P<0.005
log FC
0.0
-0.5
-1.0
-1.5
-2.0
-2.5
NPPA
MYL7
SCN5A
ATP2A2
MYL4
RYR2

Fig. 3: Altered promoter-enhancer interactions in *LMNA-S143P* iPSC-aCMs at AF-associated genes. a. Positive correlation between enhancer accessibility and differential expression of target genes. **b.** Gene enrichment analysis of target genes associated with differentially accessible enhancers. **c.** *ATAC*-seq and *RNA*-seq fold changes of target genes linked to differentially accessible enhancers. ($FDR < 0.05$, $log2\ FC > 0$ three replicates of each group) **d-g.** Promoter interactions for *GATA4*, *GATA6*, *TBX5*, and *NPPA*. Dark purple arcs indicate enhancer interactions with significant changes in accessibility. **h.** Significant downregulation of *TBX5* transcriptional targets from RNA sequencing.

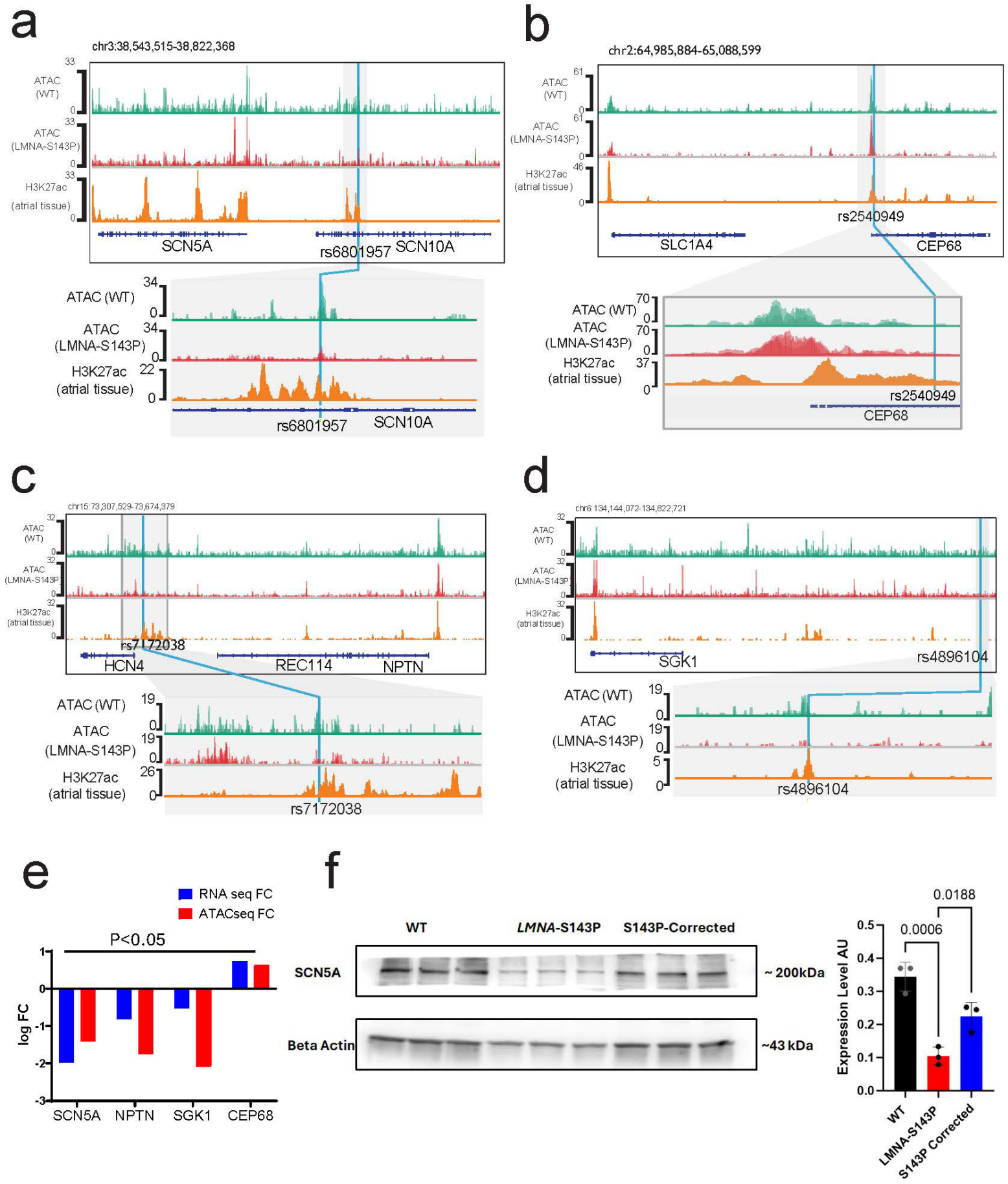
a
chr3:38,543,515-38,822,368
ATAC (WT)
ATAC (LMNA-S143P)
H3K27ac (atrial tissue)
SCN5A
rs6801957
SCN10A
b
chr2:64,985,884-65,088,599
rs2540949
SLC1A4
CEP68
c
chr15:73,307,529-73,674,379
rs7172038
HCN4
REC114
NPTN
d
chr6:134,144,072-134,822,721
SGK1
rs4896104
e
RNA seq FC
ATACseq FC
P<0.05
log FC
SCN5A
NPTN
SGK1
CEP68
f
WT
LMNA-S143P
S143P-Corrected
SCN5A
~ 200kDa
Beta Actin
~43 kDa
0.0188
0.0006
Expression Level AU
WT
LMNA-S143P
S143P Corrected

Fig. 4: Altered chromatin accessibility in AF risk loci in *LMNA*-S143P iPSC-aCMs. **a-d.** Genome Viewer ATAC and H3K27ac tracks showing altered chromatin accessibility in *LMNA*-S143P iPSC-aCMs at AF-associated loci identified by GWAS in non-coding genomic regions, including enhancer regions harboring SNPs rs6801957, rs2540949, rs7172038, and rs4896104. **e.** Differentially expressed target genes of AF-associated loci overlapping with differential ATAC peaks in regulatory regions. **f.** Validation of *SCN5A* downregulation and rescue by CRISPR correction of the mutation (n=3 representative of three independent differentiations. Ordinary one-way ANOVA with multiple comparisons $p<0.05$). Significant peaks are indicated at $Q < 0.05$, $\log2FC > 0$.

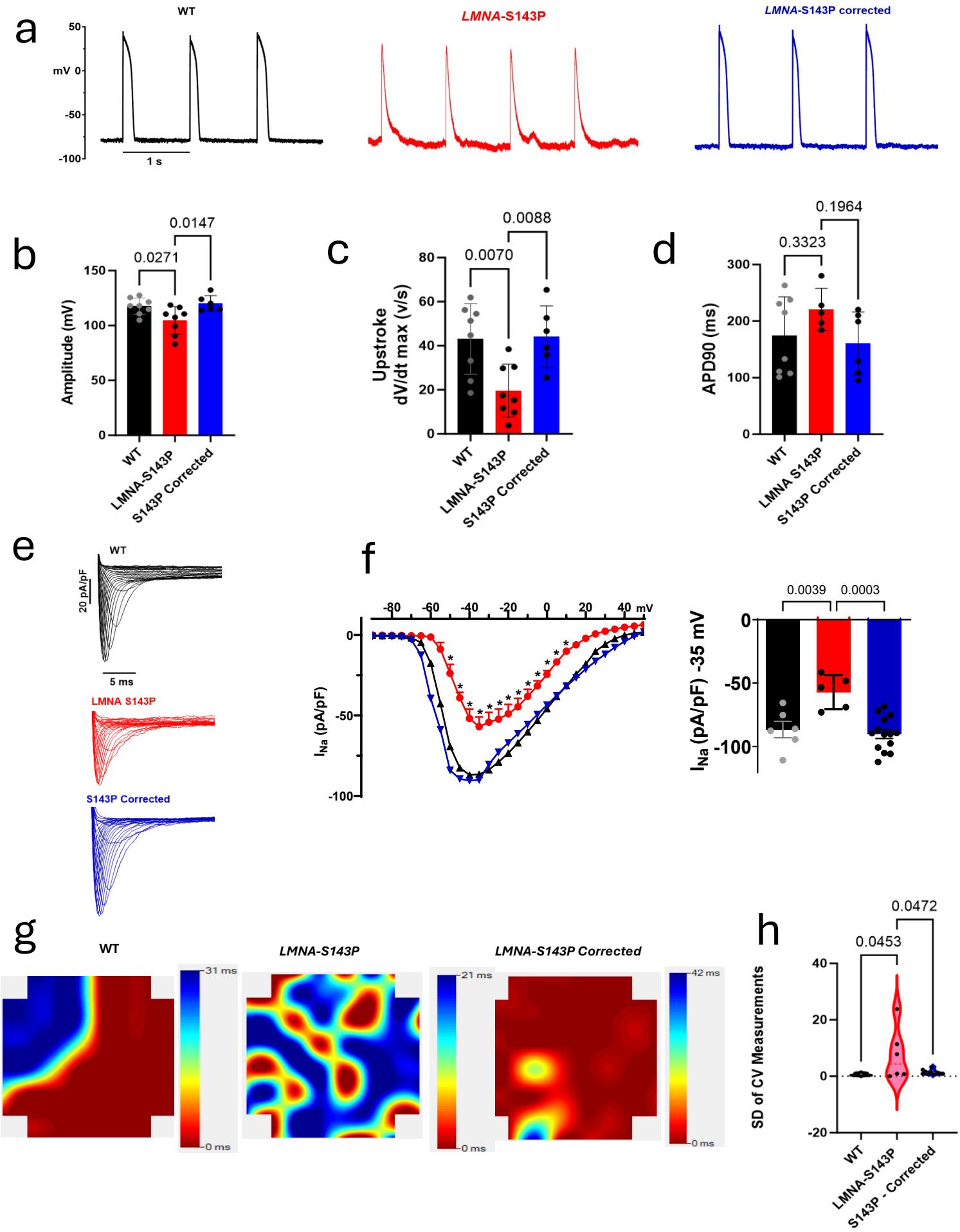
a
WT
LMNA-S143P
LMNA-S143P corrected
mV
1 s
b
Amplitude (mV)
0.0271
0.0147
WT
LMNA-S143P
S143P Corrected
c
Upstroke dV/dt max (v/s)
0.0070
0.0088
d
APD90 (ms)
0.3323
0.1964
e
20 pA/pF
5 ms
LMNA S143P
S143P Corrected
f
mV
I_{Na} (pA/pF)
I_{Na} (pA/pF) -35 mV
0.0039
0.0003
g
31 ms
0 ms
21 ms
42 ms
h
SD of CV Measurements
0.0453
0.0472
S143P - Corrected

Fig. 5: Electrophysiological alterations in *LMNA-S143P* iPSC-aCMs. a-b. Representative evoked action potential (AP) traces measured by whole-cell patch clamping show reduced AP amplitude in *LMNA-S143P* iPSC-aCMs, which is rescued by *LMNA-S143P* corrected iPSC-aCMs. **c.** Reduced upstroke velocity/instantaneous rate of voltage change over time (dV/dTmax), an indicator of atrial conduction velocity, in *LMNA-S143P* iPSC-aCMs. **d.** No change in action potential duration at 90% repolarization (*APD90*). **e.** Representative sodium current (I_{Na}) traces show reduced sodium current density in *LMNA-S143P* iPSC-aCMs. **f.** The current-voltage (*I/V*) curve shows reduced *INa* in *LMNA-S143P* iPSC-aCMs, quantified in the bar graph. (*a-d*, n = 5-7 cells per group, from three independent differentiations). (*Ordinary one-way ANOVA with multiple comparisons p<0.05*). **g.** Activation maps of propagation of electrical activity measured by a multielectrode array (MEA) show marked conduction heterogeneity in *LMNA-S143P* iPSC-aCMs (n = 6 stimulated conduction velocity [CV] measurements for each group). **h.** Increased standard deviation (SD) of conduction velocity measurements in *LMNA-S143P* iPSC-aCMs. (Ordinary one-way ANOVA with multiple comparisons p<0.05).

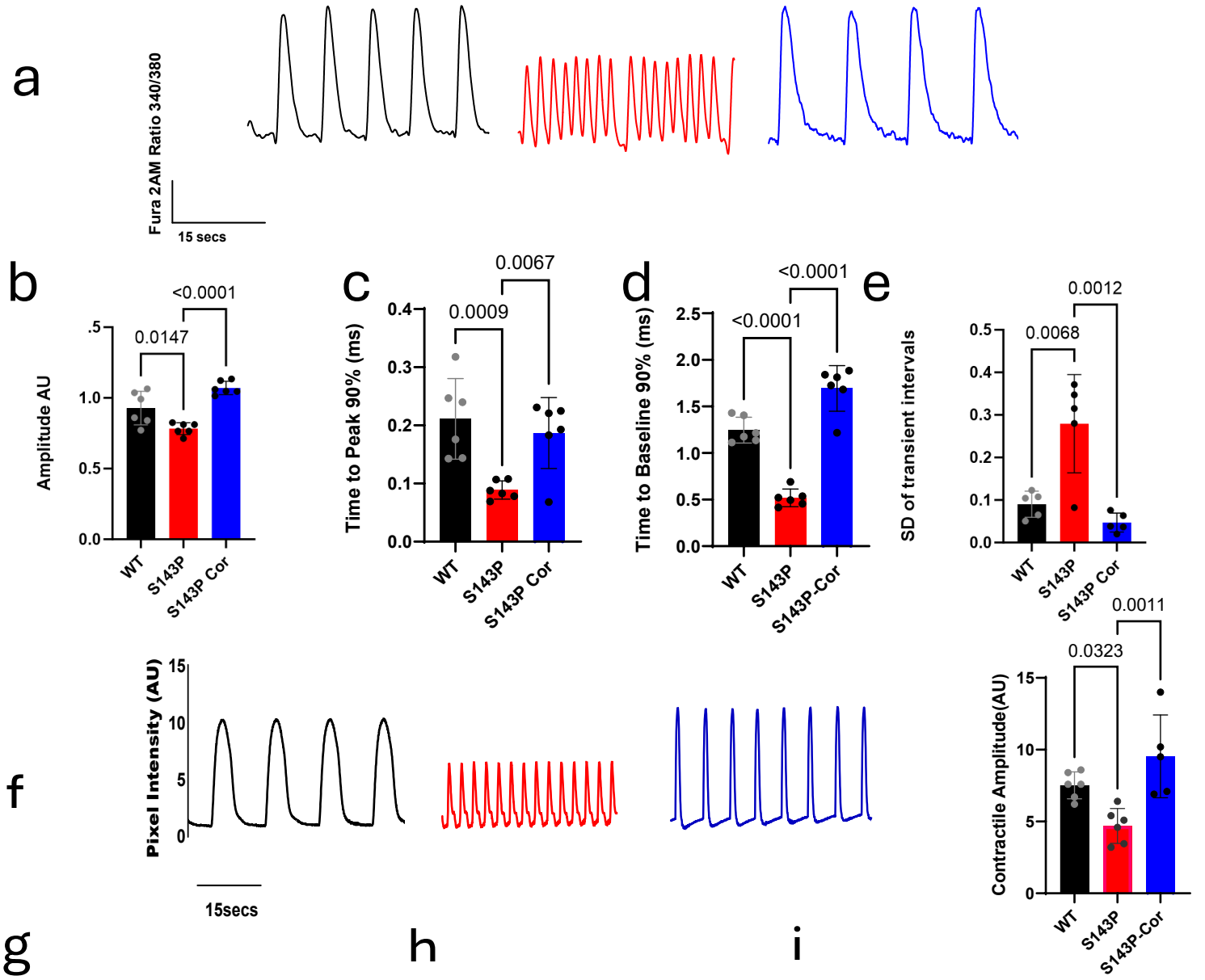

g h i

WT

LMNA-S143P

Fig. 6: Calcium transient aberrations and decreased contractility in *LMNA-S143P* iPSC-aCMs. a-e. Representative traces of calcium transients showing reduced amplitude, shorter time to peak, delayed time to relaxation, and irregularity of transient intervals in *LMNA-S143P* iPSC-aCMs, which are rescued by CRISPR correction of the mutation. **f.** Reduced contractile amplitude in *LMNA-S143P* iPSC-aCMs. **g-i.** Transmission electron microscopy images showing features of atrial myopathy in *LMNA-S143P* iPSC-aCMs. **g.** Pleiomorphic nuclei, wider intermembrane space, and more heterochromatic foci (Scale = 1 μm, 12,000x magnification). **h.** Disorganized sarcomeres and thinner myofibrils (Scale = 1 μm, 15,000x magnification). **i.** Disrupted intercalated discs (Scale = 500 nm, 30,000x magnification). **b-f** n=4-6 recordings representative of three independent differentiations, Ordinary one-way ANOVA with multiple comparisons, $p<0.05$.

a

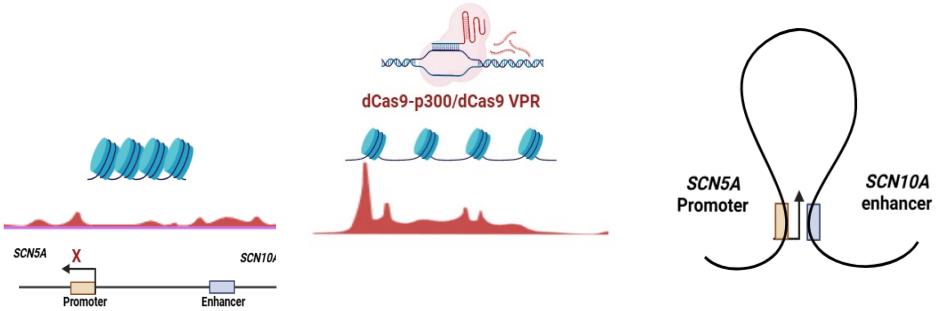
dCas9-p300/dCas9 VPR
SCN5A
X
SCN10A
Promoter
Enhancer
SCN5A
Promoter
SCN10A
enhancer

b

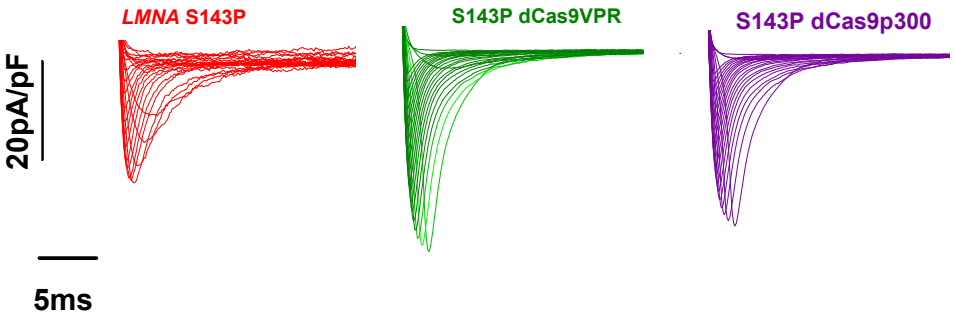
LMNA S143P
S143P dCas9VPR
S143P dCas9p300
20pA/pF
5ms

c

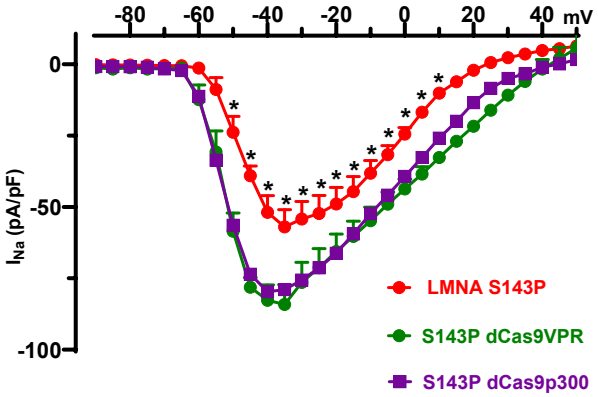
-80
-60
-40
-20
0
20
40 mV
0
-50
-100
INa (pA/pF)
LMNA S143P
S143P dCas9VPR
S143P dCas9p300

d

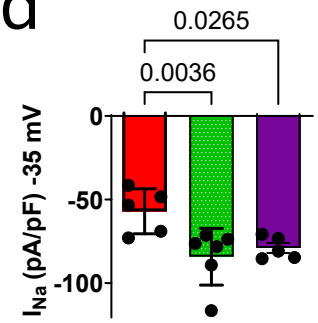
0.0265
0.0036
0
-50
-100
INa (pA/pF) -35 mV

e

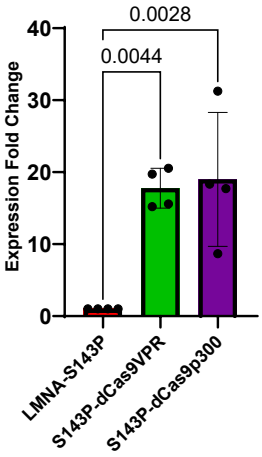
0.0028
0.0044
40
30
20
10
0
Expression Fold Change
LMNA-S143P
S143P-dCas9VPR
S143P-dCas9p300

Fig. 7: CRISPR activation of SCN5A restores INa in *LMNA-S143P* iPSC-aCMs. a. Schematic showing the CRISPR activation design. A closed chromatin conformation at the SCN5A-SCN10A locus inhibits transcription of SCN5A. RNA-guided binding of dCas9-VPR at the SCN5A promoter and dCas9-p300/CBP histone acetyltransferase at the SCN10A enhancer region initiates transcription of SCN5A. **b.** Representative INa traces show restoration of sodium current after CRISPR activation. **c.** Current-voltage (I/V) curve showing reduced INa in *LMNA-S143P* iPSC-aCMs, rescued by transfection of CRISPR activation complexes. **d.** Current-voltage (I/V) curve quantified in a bar graph. (n = 4-6 cells per group; unpaired t-test with Welch's correction $p<0.05$). **e.** CRISPR activation restores expression of *SCN5A*; bar graph quantifying changes in expression by qPCR. n=4 replicates representative of three independent differentiations, ordinary one way ANOVA with multiple comparisons, $p<0.05$)

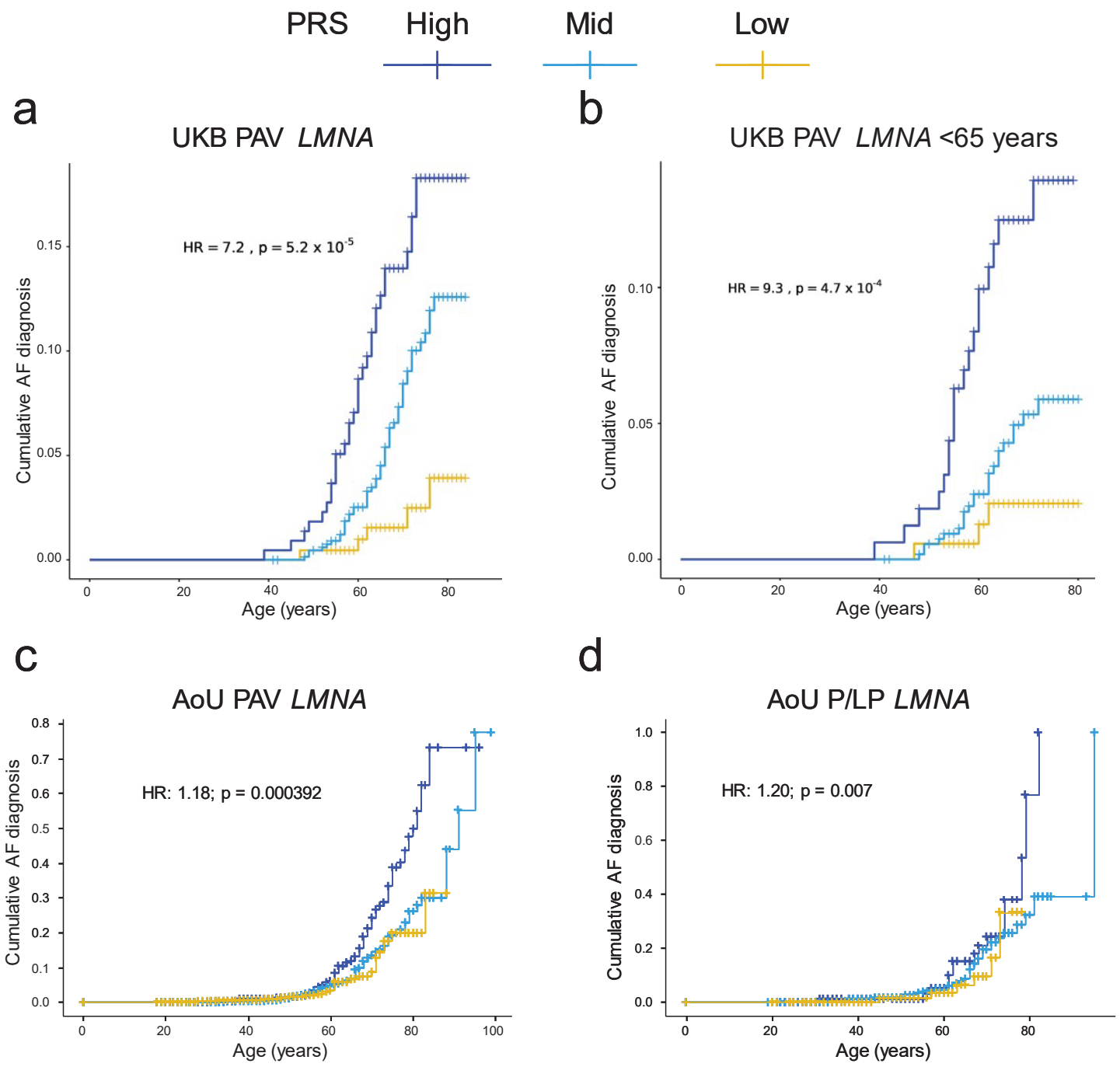
PRS
High
Mid
Low
a
UKB PAV LMNA
HR = 7.2 , p = 5.2 x 10-5
Cumulative AF diagnosis
Age (years)
b
UKB PAV LMNA <65 years
HR = 9.3 , p = 4.7 x 10-4
Cumulative AF diagnosis
Age (years)
c
AoU PAV LMNA
HR: 1.18; p = 0.000392
Cumulative AF diagnosis
Age (years)
d
AoU P/LP LMNA
HR: 1.20; p = 0.007
Cumulative AF diagnosis
Age (years)

Fig. 8: Risk of AF in the UK Biobank (UKB) and All of Us (AoU) cohorts by polygenic risk score (PRS) category. a Risk of AF in carriers of protein-altering variants (PAVs) in *LMNA* in the UK Biobank by PRS category (n = 1,109). The risk of AF is doubled in *LMNA* PAV carriers compared to non-LMNA PAV carriers (Supplementary Fig. 9a). **b.** Risk of AF in young (<65 years) participants in the UKB with PAVs in *LMNA* by PRS category is doubled compared to non-*LMNA* PAV carriers (Supplementary Fig. 9b) **c.** Risk of AF in carriers of PAV in *LMNA* by PRS category in the AoU cohort (n = 2,511). A higher PRS is significantly associated with an elevated risk of AF in cases (those with AF) compared to controls (those without AF). **d.** Risk of AF in carriers of Pathogenic/Likely Pathogenetic (P/LP) *LMNA* variants in the AoU cohort by PRS category (n = 510). A significantly higher risk is observed in cases.

SUPPLEMENTAL DATA

Fig. S1 iPSC Validation and Sanger Sequencing

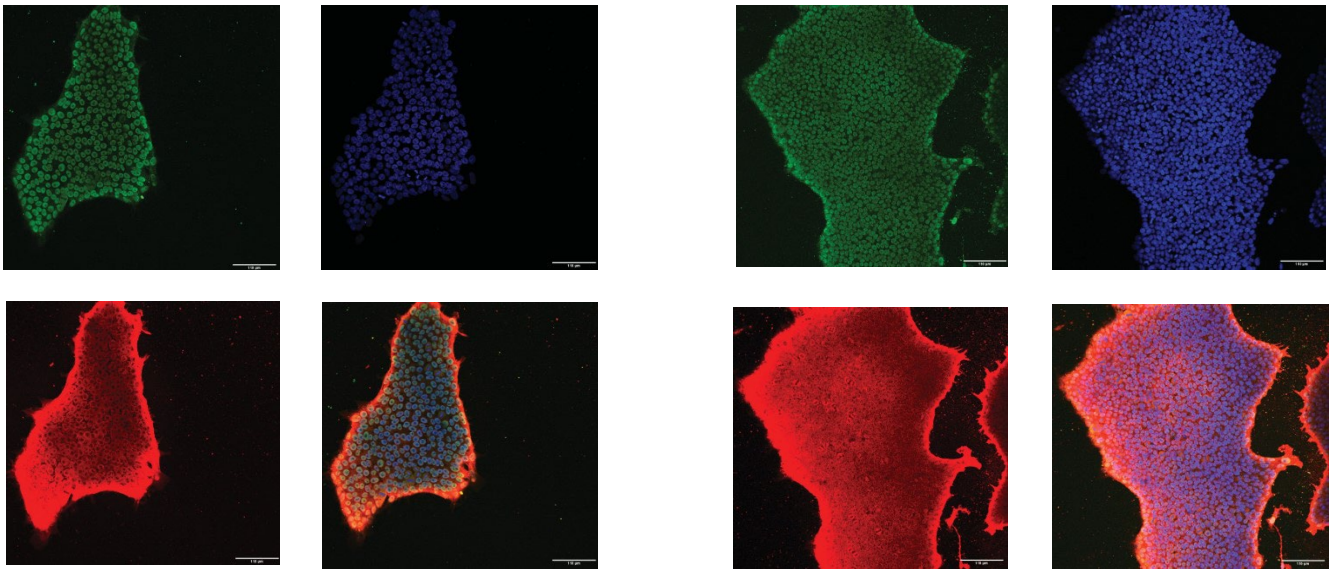

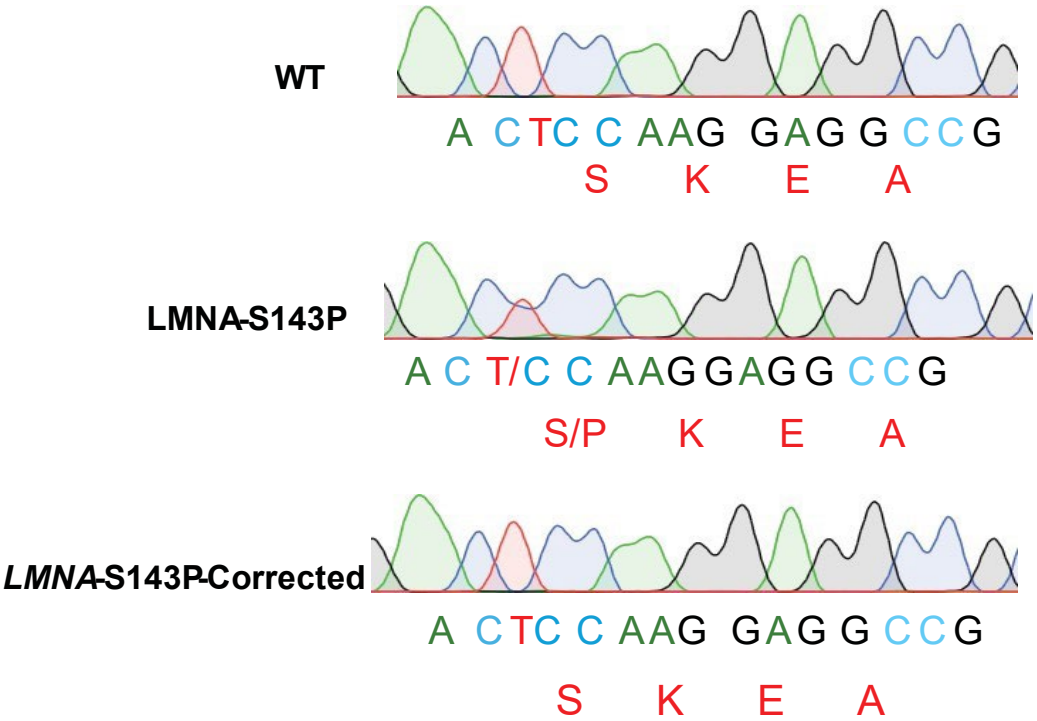

Supplementary Fig. 1: **iPSC Validation and Sanger Sequencing. a,** Immunostaining of pluripotency markers OCT4 and SOX2 in iPSCs. **b,** Sanger sequencing showing heterozygous missense variant at position 427 T>C resulting in an amino acid change from Serine to Proline.

a

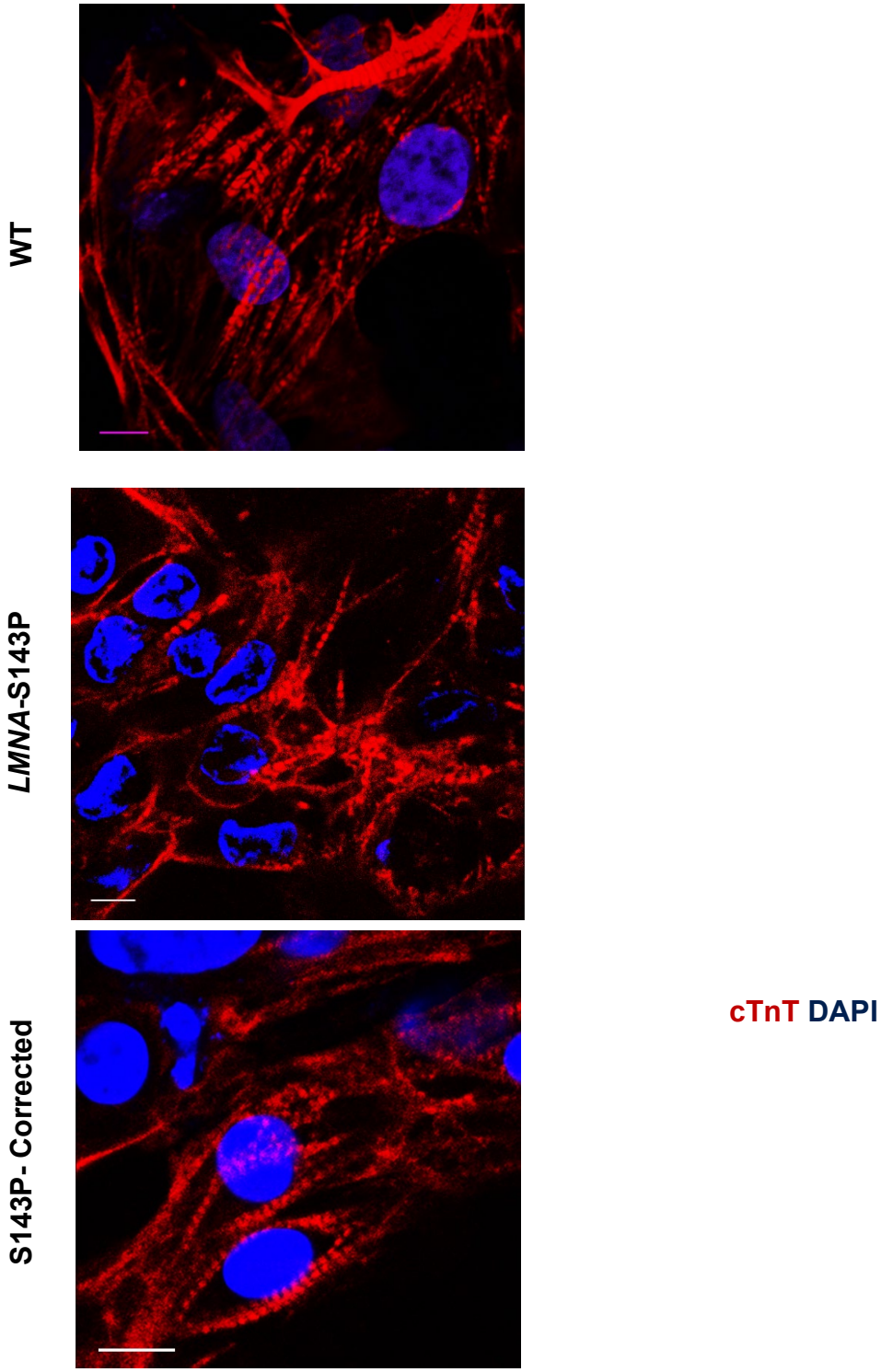

b

Videos of beating iPSC aCMs

Supplementary Fig. 2: Immunostaining of iPSC-aCMs for cardiac troponin T. a, cTnT in red and DAPI in blue. **b,** Videos of beating iPSC-aCMs.

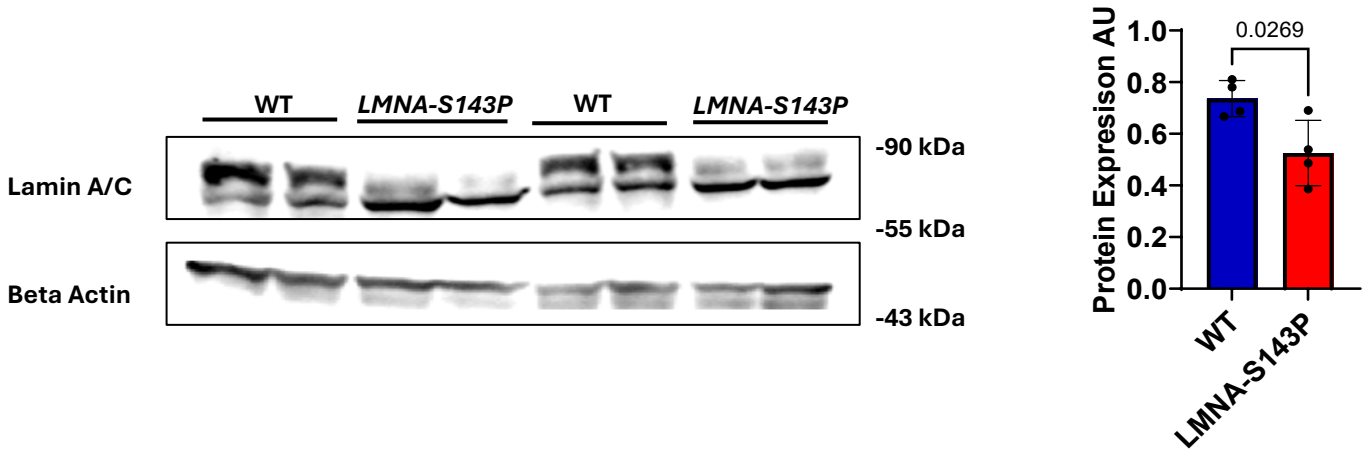

Supplementary Fig. 3: Protein expression of Lamin A/C isoforms in wild-type (WT) and *LMNA*-S143P iPSC-aCMs.

a

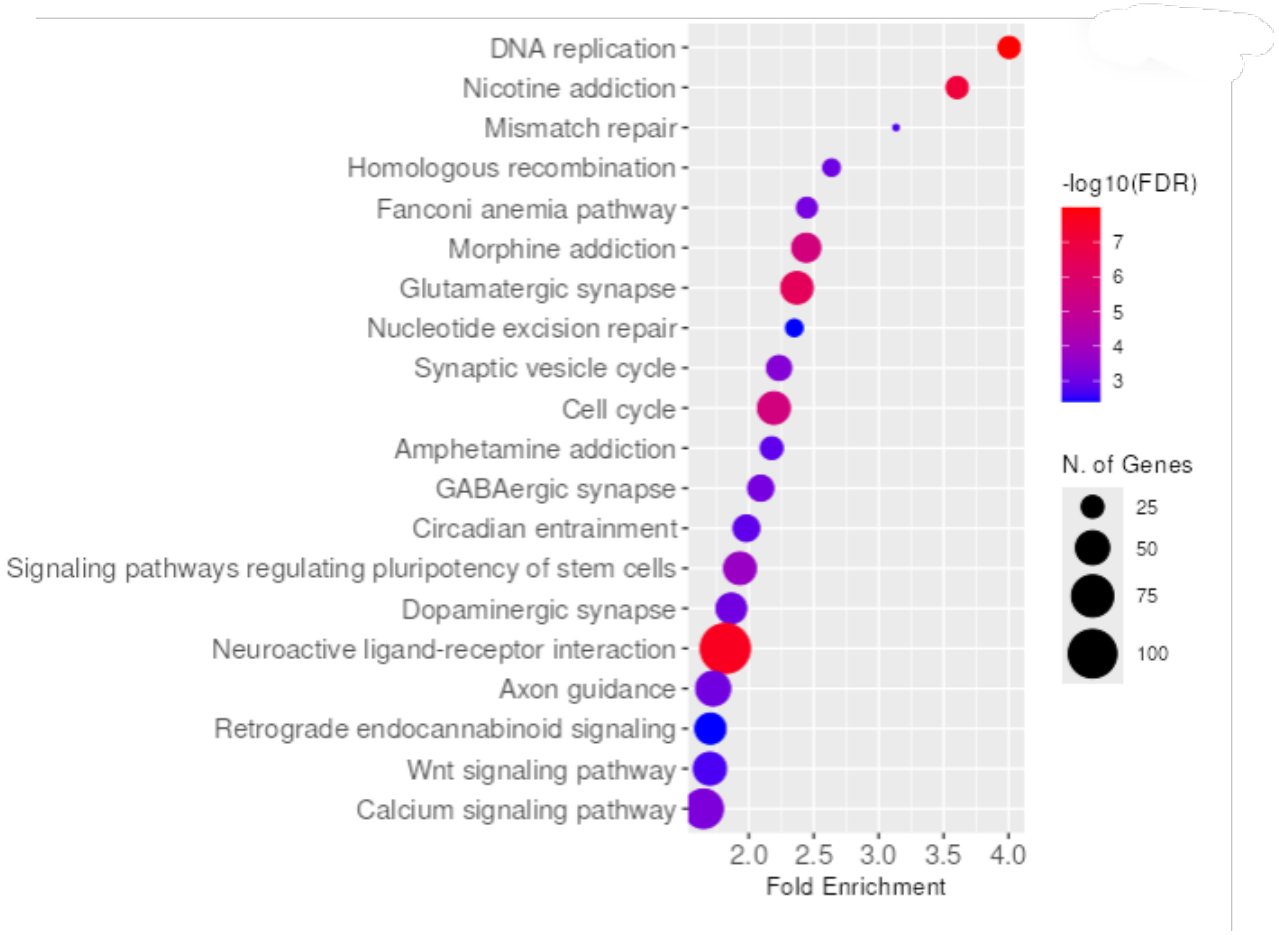
DNA replication
Nicotine addiction
Mismatch repair
Homologous recombination
Fanconi anemia pathway
Morphine addiction
Glutamatergic synapse
Nucleotide excision repair
Synaptic vesicle cycle
Cell cycle
Amphetamine addiction
GABAergic synapse
Circadian entrainment
Signaling pathways regulating pluripotency of stem cells
Dopaminergic synapse
Neuroactive ligand-receptor interaction
Axon guidance
Retrograde endocannabinoid signaling
Wnt signaling pathway
Calcium signaling pathway
2.0
2.5
3.0
3.5
4.0
Fold Enrichment
-log10(FDR)
7
6
5
4
3
N. of Genes
25
50
75
100

b

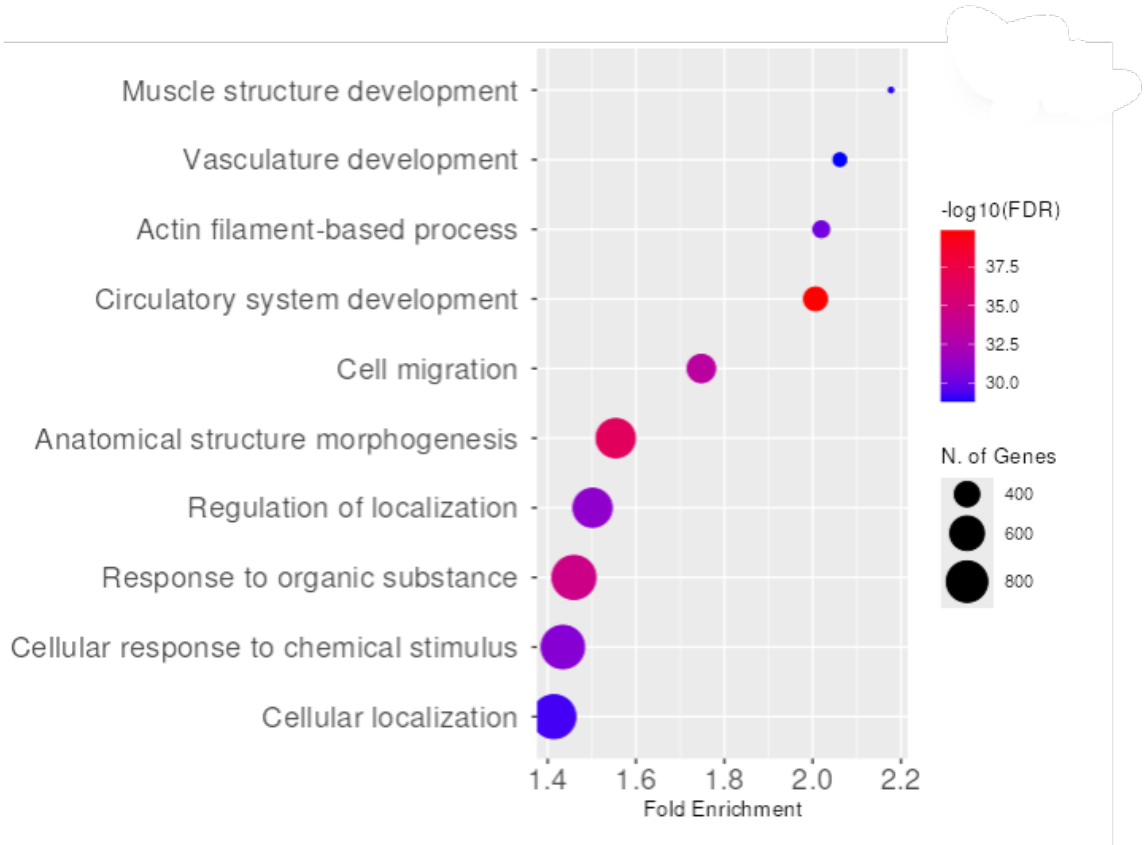
Muscle structure development
Vasculature development
Actin filament-based process
Circulatory system development
Cell migration
Anatomical structure morphogenesis
Regulation of localization
Response to organic substance
Cellular response to chemical stimulus
Cellular localization
1.4
1.6
1.8
2.0
2.2
Fold Enrichment
-log10(FDR)
37.5
35.0
32.5
30.0
N. of Genes
400
600
800

C

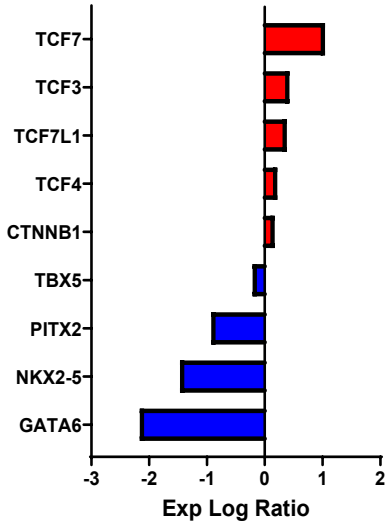

Supplementary Fig. 4: Transcriptomic changes in *LMNA*-S143P iPSC-aCMs. a-b, KEGG Pathway enrichment analysis of upregulated genes. **b,** GO enrichment analysis of downregulated genes. **c,** Transcription Factor enrichment analysis**,** e.g., Differential expression at Q < 0.05, log2FC > 0.

a

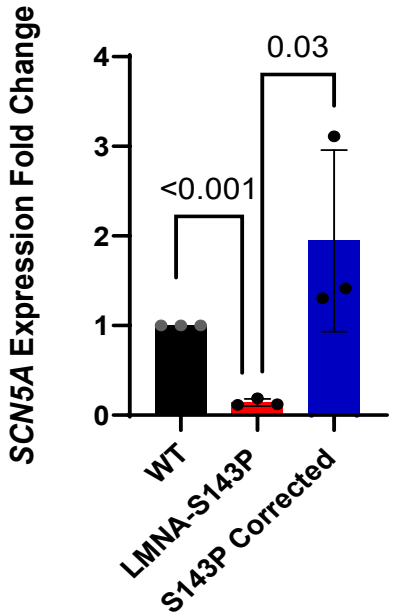
SCN5A Expression Fold Change
4
3
2
1
0
0.03
<0.001
WT
LMNA-S143P
S143P Corrected

b

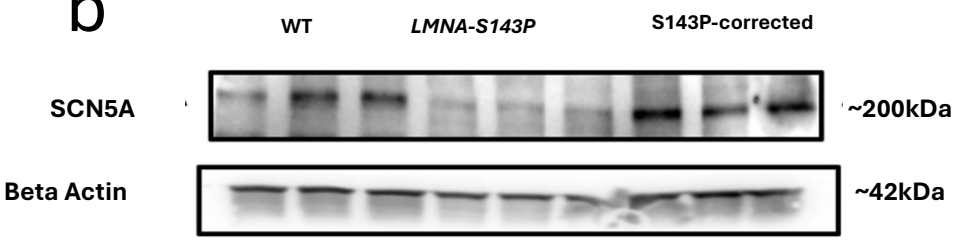
WT
LMNA-S143P
S143P-corrected
SCN5A
~200kDa
Beta Actin
~42kDa

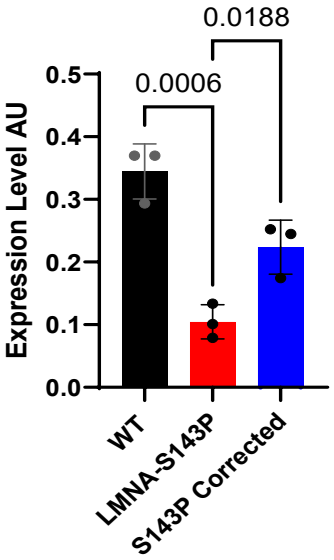
Expression Level AU
0.5
0.4
0.3
0.2
0.1
0.0
0.0006
0.0188
WT
LMNA-S143P
S143P Corrected

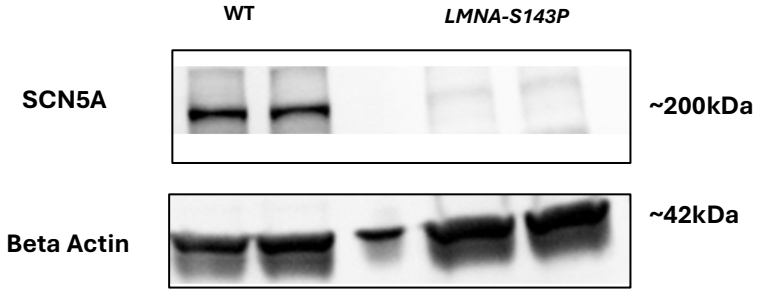
WT
LMNA-S143P
SCN5A
~200kDa
Beta Actin
~42kDa

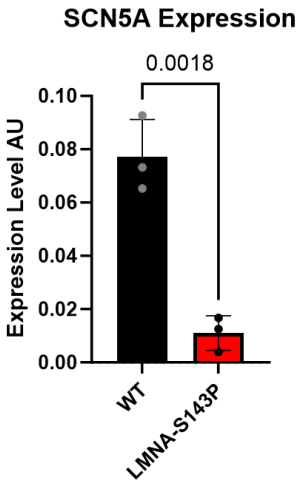
SCN5A Expression
Expression Level AU
0.10
0.08
0.06
0.04
0.02
0.00
0.0018
WT
LMNA-S143P

Supplementary Fig. 5: a. Reduced mRNA expression of *SCN5A* in *LMNA*-S143P iPSC-aCMs by qPCR. **b.** Reduced protein expression of *SCN5A* in *LMNA*-S143P iPSC-aCMs in samples from multiple differentiations.

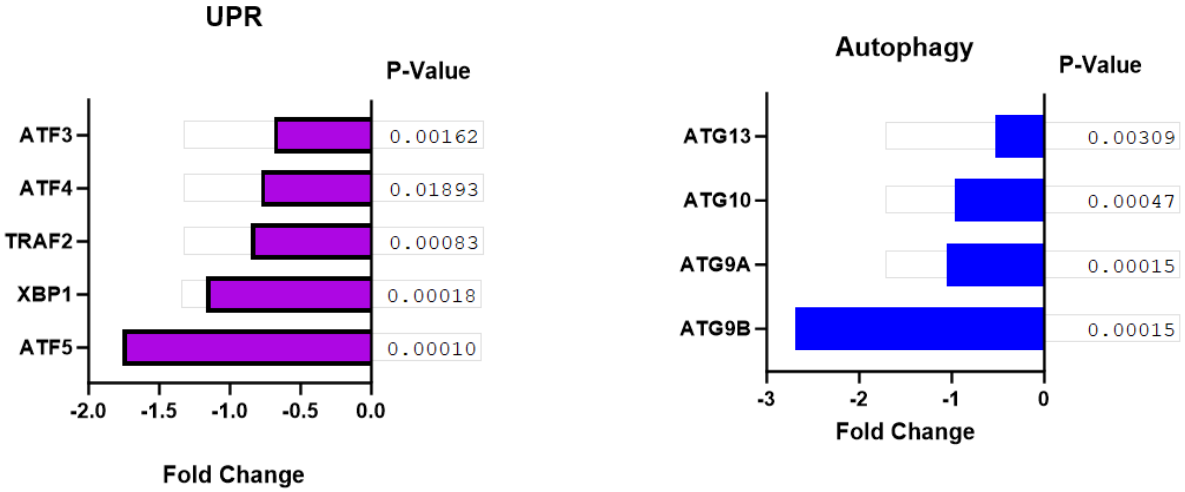

Supplementary Fig. 6: Expression fold change of genes involved in (a) Unfolded Protein Response (UPR) and (b) Autophagy (ATG) in *LMNA*-S143P iPSC-aCMs.

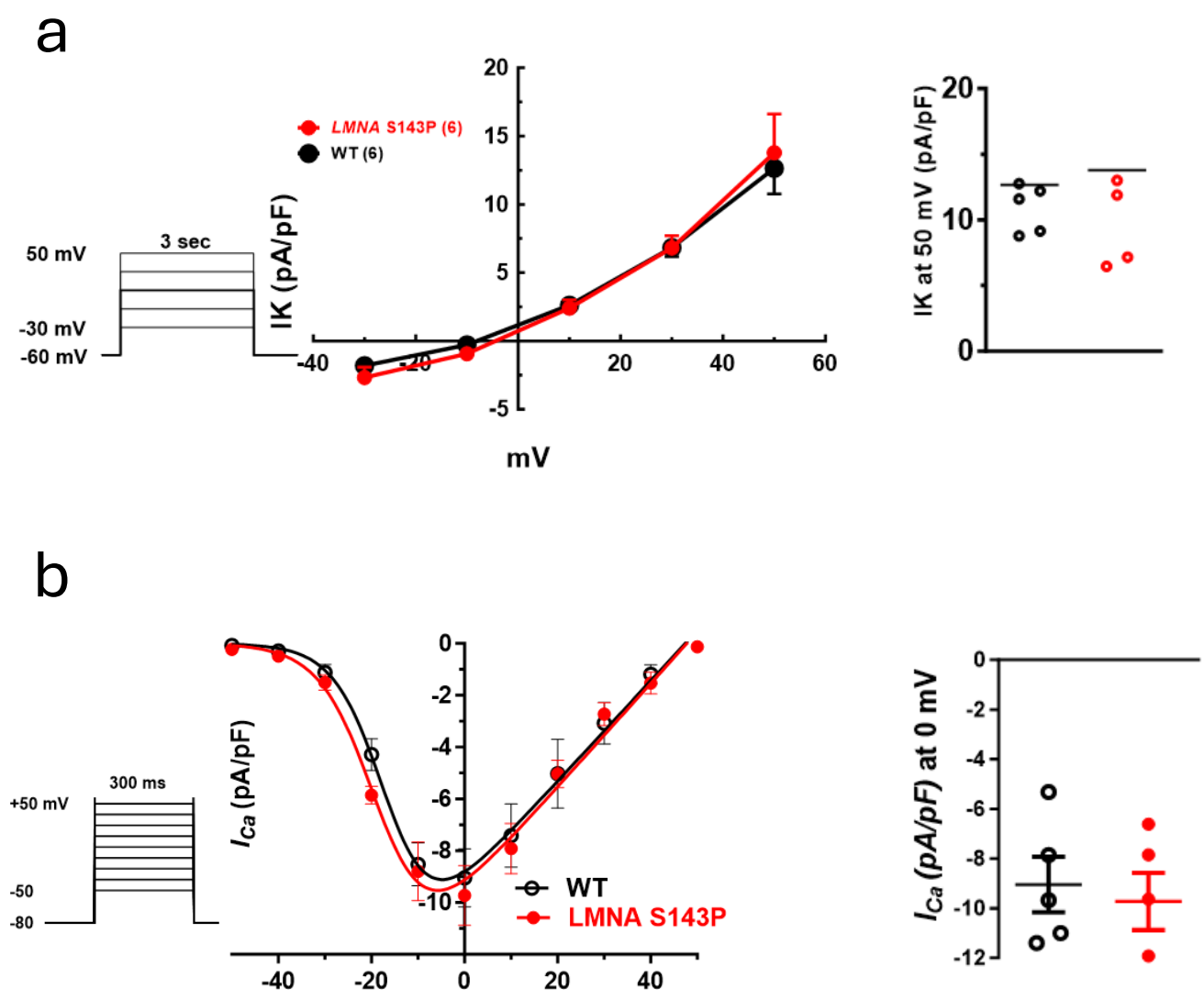

Supplementary Fig. 7: *LMNA*-S143P does not alter potassium (I_K) or calcium ($I_{Ca,L}$) currents. a, IV relationship for I_K in WT, *LMNA*-S143P iPSC-aCMs. **b,** IV relationship for I_{CaL} in the two groups.

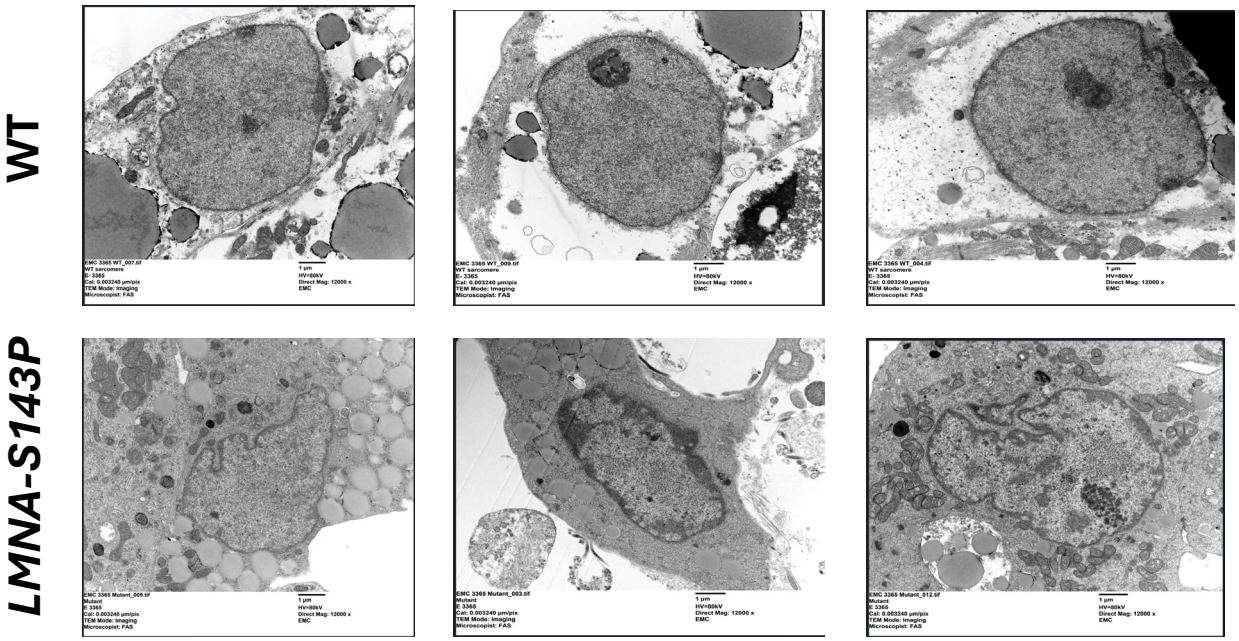

Supplementary Fig. 8: Transmission electron microscopy shows nuclear deformities in *LMNA*-S143P iPSC-aCMs.

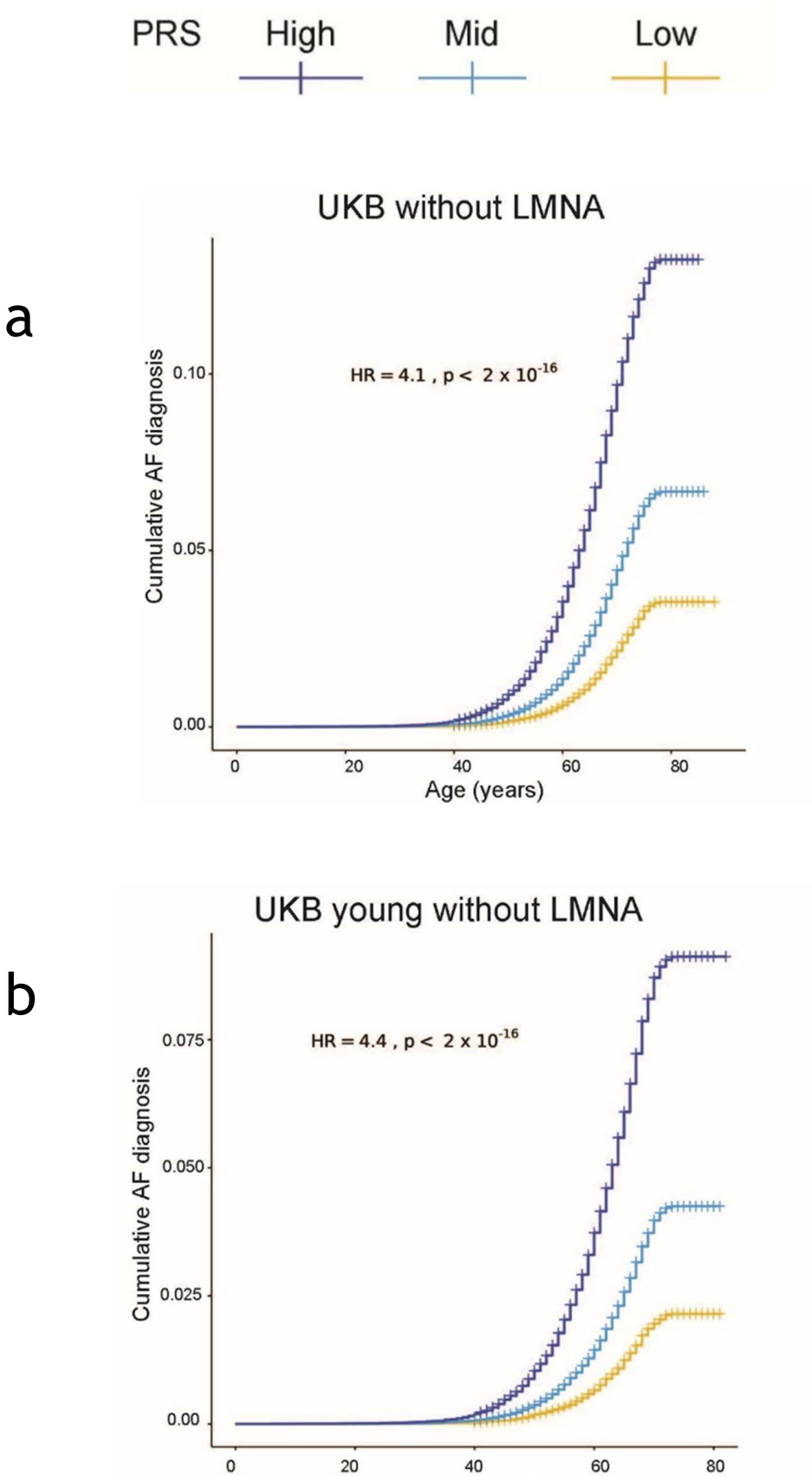
PRS
High
Mid
Low
a
UKB without LMNA
HR = 4.1 , p < 2 x 10^-16
Cumulative AF diagnosis
0.10
0.05
0.00
0
20
40
60
80
Age (years)
b
UKB young without LMNA
HR = 4.4 , p < 2 x 10^-16
Cumulative AF diagnosis
0.075
0.050
0.025
0.00
0
20
40
60
80

Supplementary Fig.9. AF prevalence without PAV in *LMNA.* a Risk of AF in individuals who do not harbor PAVs in *LMNA* in the UK Biobank by PRS category (n = 419,087). A higher PRS is associated with a higher risk of AF in general. **b.** Risk of AF in young (<65 years) participants in the UKB who do not harbor PAVs in *LMNA* by PRS category.

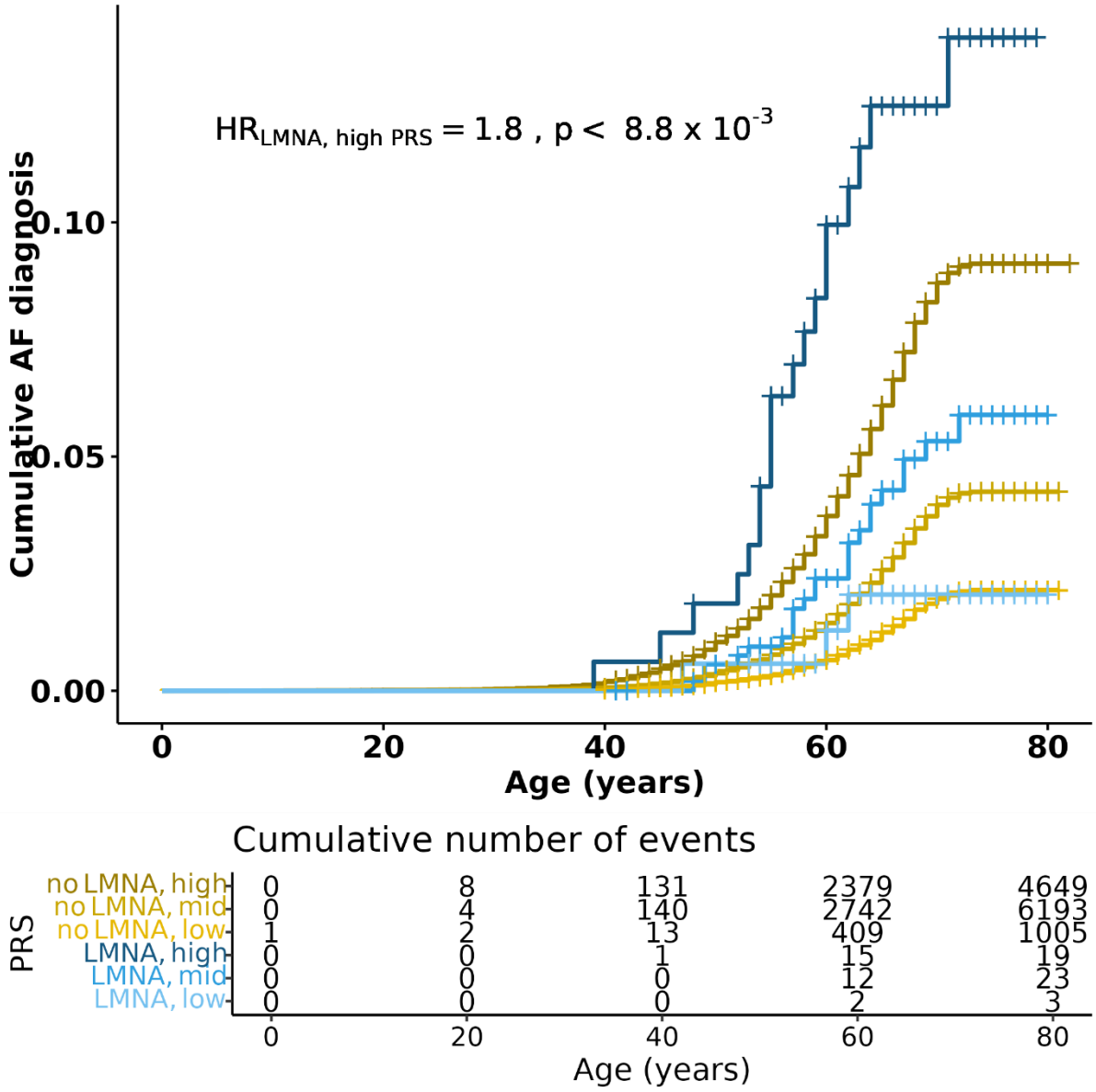

Supplementary Fig. 10: Risk of AF in the young (<65 years) UK Biobank participants using non-*LMNA* carriers with high PRS as the reference group.

LMNA: LMNA carriers, nLMNA: non-LMNA carriers, low: low-risk AF PRS, mid: medium-risk AF PRS, high: high-risk AF PRS.

Supplementary Table 1: Overlap of AF risk loci and ATAC peaks in *LMNA*-S143P iPSC-aCMs.

rsID	rsID:Nearest_Gene(s)†	Chromosome	log2FC	p-value
rs4896104	ALDH8A1	chr6	-2.07327	0.004304
rs55734480	DGKB	chr7	-1.9301	0.008852
rs7172038	NEO1	chr15	-1.73881	0.009063
rs6801957	SCN10A	chr3	-1.40184	0.00035
rs1769758	ZMIZ1	chr10	-1.38549	3.73E-05
rs2540949	CEP68	chr2	0.634214	0.000908
rs12640611	WDR1	chr4	2.067337	8.50E-09
rs1886512	KLF12	chr13	2.179281	0.002199

Supplementary Table 2: Risk of AF in UK Biobank participants who do not harbor a PAV in *LMNA* by PRS category (n=419,087).

	No AF	Has AF	HR (p-value)
Low PRS (bottom 20%)	81246	1881	1.00
Mid PRS (20-80%)	240175	11178	1.94 ($p < 2 \times 10^{-16}$)
High PRS (top 20%)	76749	7860	4.11 ($p < 2 \times 10^{-16}$)

Supplementary Table 3: Risk of AF in carriers of PAVs in *LMNA* in the UK Biobank by PRS category (n=1,109).

	No AF	Has AF	HR (p-value)
Low PRS (bottom 20%)	216	5	1.00
Mid PRS (20-80%)	617	52	3.54 ($p = 7.49 \times 10^{-3}$)
High PRS (Top 20%)	187	32	7.18 ($p = 5.15 \times 10^{-5}$)

Supplementary Table 4: Risk of AF in young (<65 years) in *LMNA* PAV carriers compared to non-*LMNA* carriers.

	No AF	Has AF	HR (p-value)
Non-*LMNA* carriers	320470	11847	1.56 ($p = 3.01 \times 10^{-3}$)
LMNA carriers	823	45	

Supplementary Table 5: Risk of AF in the young (< 65 yo) UK Biobank non-*LMNA* carriers by PRS category

	No AF	Has AF	HR (p-value)
Low PRS (bottom 20%)	64842	1005	1.00
Mid PRS (20-80%)	193150	6193	1.96 ($p < 2 \times 10^{-16}$)
High PRS (top 20%)	62478	4649	4.4 ($p < 2 \times 10^{-16}$)

Supplementary Table 6: Risk of AF in young (<65 years) in UK Biobank PAVs in LMNA carriers by PRS category.

	No AF	Has AF	HR (p-value)
Low PRS (bottom 20%)	170	3	1.00
Mid PRS (20-80%)	511	23	3.08 ($p = 7.11 \times 10^{-2}$)
High PRS (top 20%)	142	19	9.31 ($p = 4.73 \times 10^{-4}$)

Supplementary Table 7: Risk of AF in UK Biobank P/LP LMNA carriers by PRS category.

	No AF	Has AF
Low PRS (bottom 20%)	5	0
Mid PRS (20-80%)	17	2
High PRS (top 20%)	9	4